Teleconnections in the Geopotential Height Field during the Northern Hemisphere Winter[1]

JOHN M. WALLACE AND DAVID S. GUTZLER[2]

Department of Atmospheric Sciences, University of Washington, Seattle 98195

(Manuscript received 11 August 1979, in final form 8 September 1980)

ABSTRACT

Contemporaneous correlations between geopotential heights on a given pressure surface at widely separated points on earth, referred to as teleconnections in this paper, are studied in an attempt to identify and document recurrent spatial patterns which might be indicative of standing oscillations in the planetary waves during the Northern Hemisphere winter, with time scales on the order of a month or longer. A review of existing literature on the subject reveals the existence of at least four such patterns: the North Atlantic and North Pacific Oscillations identified by Walker and Bliss (1932), a zonally symmetric seesaw between sea level pressures in polar and temperature latitudes, first noted by Lorenz (1951), and what we will refer to as the Pacific/North American pattern, which has been known to operational long-range forecasters in this country since the 1950's.

A data set consisting of NMC monthly mean sea level pressure and 500 mb height analyses for a 15-year period is used as a basis for calculating the temporal correlation coefficients between all possible pairs of grid points. An objective method is used to identify and describe the strongest teleconnection patterns in this correlation matrix. The five leading patterns are compared with, and found to bear some similarity to, the leading eigenvectors of the correlation matrix. Certain of the above calculations are repeated on an independent data set in order to test the reproducibility of the patterns.

The North Atlantic Oscillation and the Pacific/North American patterns are strongly evident in both data sets. The former is associated with fluctuations in the strength of the climatological mean jet stream over the western Atlantic. The Pacific/North American pattern includes a north–south seesaw in the central Pacific somewhat reminiscent of the North Pacific Oscillation mentioned by Walker and Bliss (1932) and Bjerknes (1969), together with centers of action over western Canada and the southeastern United States. Several other teleconnection patterns are revealed by the analysis of the primary data set, but are not found to be as reproducible in the independent data set.

The sea level pressure statistics are dominated by negative correlations between the polar region and temperature latitudes, whereas the 500 mb statistics are dominated by patterns of a more regional scale, which display a nearly equivalent barotropic structure with amplitudes increasing with height. Most of the regional patterns have only one or two well-defined centers of action at the earth's surface, but at mid-tropospheric levels they are more wavelike in appearance and characterized by multiple centers of action; at these levels their structure resembles that of forced stationary waves on a sphere.

1. Introduction

Significant simultaneous correlations between temporal fluctuations in meteorological parameters at widely separated points on earth, commonly referred to as teleconnections in the descriptive literature, are of considerable interest because they provide evidence concerning the transient behavior of the planetary waves. There is abundant evidence of the existence of such correlations, particularly in fluctuations with time scales of a week or longer. In a number of cases it has been possible to identify what appear to be standing wave structures with geographically fixed nodes and antinodes on the basis of multiple-correlation statistics derived from time series from a number of different stations or grid points. In this paper we will be concerned with such multiple-correlation statistics (or teleconnection patterns as they are commonly called) for the sea level pressure and 500 mb height fields. We will restrict our attention to the Northern Hemisphere extratropics during winter.

2. Review

Much of the literature on the subject of teleconnections is difficult to interrelate and synthesize because of the lack of unique or universally agreed on criteria and procedures for defining horizontal structural relationships. For example, some investigators have used time series of sea level pressure

[1] Contribution No. 580, Department of Atmospheric Sciences, University of Washington.

[2] Present affiliation: Sigma Data Services Corporation, Goddard Laboratory for Atmospheric Sciences, NASA/Goddard Space Flight Center, Greenbelt, MD 20771.

0027-0644/81/040784-29$11.25

at some particular station as a basis for correlating or compositing atmospheric data in order to define the teleconnection patterns; some have used time series of sea level pressure differences between selected pairs of stations; some have used time series consisting of linear combinations of sea-level pressure at three or more stations (e.g., as defined by eigenvector analysis); others have used time series based on parameters such as surface temperature or upper level geopotential height, or combinations of different parameters. Different investigators have used various time-averaging intervals, ranging from a few days to a season. The choice of variables and stations incorporated into these various indicators of horizontal structure has often been dictated as much by the availability of long data records as by the shape of the patterns. As a result of the wide differences in data bases and analysis approaches it is often difficult to compare the results of different studies. The statistical significance of many of the reported teleconnection patterns is difficult to assess because of the lack of an *a priori* basis for postulating the existence of the patterns.

Despite the occasional inconsistencies and dead ends that one encounters in the literature on the subject, there is convincing evidence that long-range teleconnections exist in at least a few instances. It is well established that sea level pressure in the tropics and subtropics undergoes slow, irregular fluctuations, with a characteristic time scale on the order of a year to a few years, and having a well-defined spatial pattern indicative of a standing oscillation. This so-called Southern Oscillation, first recognized by Hildebrandsson (1897), was extensively documented on a global scale in a monumental descriptive paper by Walker and Bliss (1932). The essential features of the teleconnection patterns reported by Walker and Bliss subsequently have been confirmed on the basis of more recent data in studies by Troup (1965) and Wright (1977).[3] Observational studies by Bjerknes (1969), Krueger and Gray (1969), Ramage (1975) and others, together with modeling by Rowntree (1972) have contributed valuable dynamical insights into the nature of this phenomenon.

In this paper we will be primarily concerned with teleconnection patterns at middle and high latitudes of the Northern Hemisphere. The literature provides convincing evidence of four teleconnection patterns which we will describe as (a) the North Atlantic Oscillation, (b) the North Pacific Oscillation, (c) the zonally symmetric seesaw and (d) the Pacific/North American pattern.

[3] P. B. Wright, 1977: The Southern Oscillation-patterns and mechanisms of teleconnections and persistence. Hawaii Inst. Geophys., Rep. HIG-77-13, 107 pp.

a. The North Atlantic Oscillation

The primary evidence of teleconnection patterns in the Atlantic and European sector is based on two relationships which appear to possess a high level of statistical significance: 1) a negative correlation between the severity of winters (as defined by the mean surface temperature) in the Greenland-Labrador region and northwestern Europe; and 2) a negative correlation between sea level pressure in the vicinity of the Icelandic low near 65°N and a broad east–west belt centered near 40°N and extending from the east coast of the United States to the Mediterranean.

The standing oscillation or seesaw in winter temperatures has been extensively documented in a recent article by van Loon and Rogers (1978) who cite evidence of its existence dating back into the 18th century. The teleconnection pattern in sea level pressures has been noted by many authors over the years, including Defant (1924), Walker and Bliss (1932) and Kutzbach (1970).

Walker and Bliss believed that the teleconnection patterns in surface temperature and sea level pressure were manifestations of a single phenomenon which they termed the North Atlantic Oscillation (NAO). In accordance with their perception of the phenomenon they defined an index consisting of a linear combination of surface temperature and sea level pressure data at selected stations. Positive values of their index are indicative of a strong Icelandic low, high pressure along 40°N, strong westerlies across the North Atlantic, below-normal temperatures in the Greenland-Labrador area and in the Middle East, and above-normal temperatures in the eastern United States and northwestern Europe, as illustrated schematically in Fig. 1, while negative values of the index are indicative of anomalies in the opposite sense. Walker and Bliss pointed out that these relationships are consistent with simple dynamical arguments: an abnormally deep Icelandic low should be conducive to enhanced cold advection over the Greenland-Labrador area and an enhanced southwesterly flow of mild, marine air over northwestern Europe. The corresponding positive anomalies in sea level pressures at lower latitudes over the Atlantic and Mediterranean should be accompanied by a tendency toward southerly flow and warm advection over the eastern United States and the opposite conditions over the Middle East.

The evidence presented by Walker and Bliss in support of NAO is compromised by the fact that the relationships which they described are to some extent built into their teleconnection patterns because their index of the NAO involves no less than nine different time series. In the hands of a less astute climatologist than Sir Gilbert Walker, this analysis

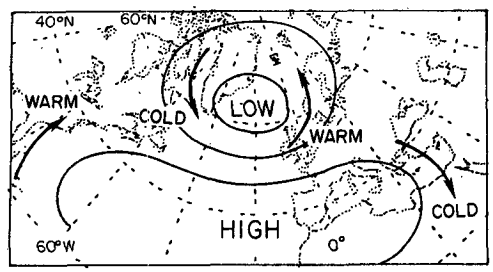

FIG. 1. Idealized relationships between pressure and temperature anomalies associated with the North Atlantic Oscillation.

procedure could well have yielded meaningless teleconnection patterns. The corroborating evidence presented by van Loon and Rogers (1978) is much more credible because their index of the oscillation is based solely on temperature differences between Greenland and Norway; the other relationships emerge spontaneously in their composite and correlation charts. Furthermore, their results have a much higher level of statistical significance by virtue of the fact that they are based on data for 46 winters (1931–76) which were not available to Walker and Bliss.

In order to further demonstrate the validity of the concept of the NAO as envisioned by the above authors we have performed the following calculation. Using a data set consisting of monthly mean, gridded sea level pressure and 700 mb height anomalies for 84 winter months (Decembers, Januarys and Februarys beginning with December 1949 and ending with February 1977), for the Northern Hemisphere,[4] we generated monthly values of the difference in 1000–700 mb thickness between two grid points located close to the stations used by van Loon and Rogers: near Jakobshavn, Greenland (70°N, 50°W) and near Oslo, Norway (60°N, 10°E). This index of the NAO was then temporally correlated with sea level pressure at every grid point over the 84 month data sample in order to produce the correlation map shown in Fig. 2. The resulting pattern strongly resembles the idealized configuration in Fig. 1 and some of the composite charts in van Loon and Rogers (1978).

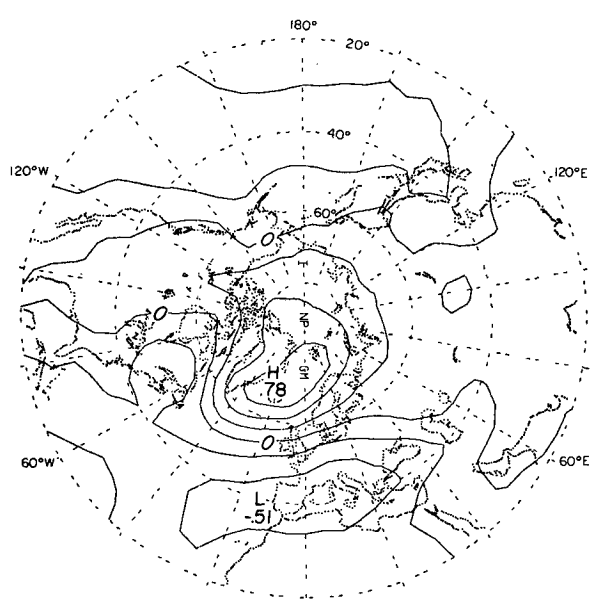

FIG. 2. 1000–700 mb thickness at 70°N, 50°W minus 1000–700 mb thickness at (60°N, 10°E), correlated with sea level pressure at every gridpoint. Based on anomalies for 84 winter months (Decembers, Januarys and Februarys for the winters 1949–50 through 1976–77). Contour interval 0.2.

van Loon and Rogers' analysis revealed another important aspect of the NAO which had not been previously noted: winters which are colder than normal in the Greenland-Labrador region and warmer than normal in northwestern Europe were found to be characterized not only by a deeper than normal Icelandic low, but also by positive sea level pressure anomalies in middle latitudes of the central North Pacific. There is some suggestion of such a relationship in Fig. 2, but it shows up much more strongly in Figs. 3 and 7 of van Loon and Rogers (1978). This result suggests that it might be possible to use some measure of the difference between the depths of the Icelandic and Aleutian lows as another index of the NAO. Fig. 3 shows the sea level pressure difference between grid points near Iceland (70°N, 20°W) and south of the Aleutians (50°N, 165°W) correlated with (a) 1000–700 mb thickness and (b) 700 mb height for all grid points, based on the same data set as Fig. 2. The resulting correlation pattern does indeed show a clear signature of NAO: the combination of a strong Icelandic low and weak Aleutian low is conducive to positive thickness anomalies over the eastern United States and northwestern Europe and negative thickness anomalies over the Greenland-Labrador region and the Middle East. Of comparable strength in the correlation pattern are the centers over the central North Pacific, near 50°N, and over western Canada. We will comment further on these features and on Fig. 3b in Section 2c.

The fact that the North Atlantic and North Pacific antinodes or centers of action in the sea level pressure pattern in the NAO correspond to centers of high variability of sea level pressure suggests that this pattern might reflect a preferred mode of variability of the sea level pressure field. van Loon

[4] The data were obtained on magnetic tape from the NCAR data library. Before further processing, the 28-year means for each calendar month were removed from the data. Hence, the correlations referred to in this paper reflect the influence of year-to-year variability of the wintertime means, and month-to-month variability within the same winter, but they do not include any effects of the annual cycle.

and Rogers (1976) pointed out the rather striking similarity between the sea level pressure pattern associated with the NAO (their Figs. 3 and 7) and the first eigenvector derived from 66 unnormalized January mean sea level pressure anomaly fields by Kutzbach (1970). We have attempted to reproduce Kutzbach's results using our own eigenvector analysis routines on his data set, and on the 84-month data set used in Figs. 2 and 3. The resulting patterns, shown in Fig. 4, are similar to Kutzbach's, but there is somewhat greater emphasis on the center of action over the polar region because the grid that we used includes data at 80°N, and our analysis extends over the polar cap. This slight change in emphasis gives our pattern a more zonally symmetric appearance than Kutzbach's, so that the center of action near Iceland does not stand out as clearly. Hence, despite the similarities that have been pointed out, we are not fully convinced that there is a one-to-one correspondence between the NAO and the first eigenvector of wintertime sea level pressure anomaly patterns.

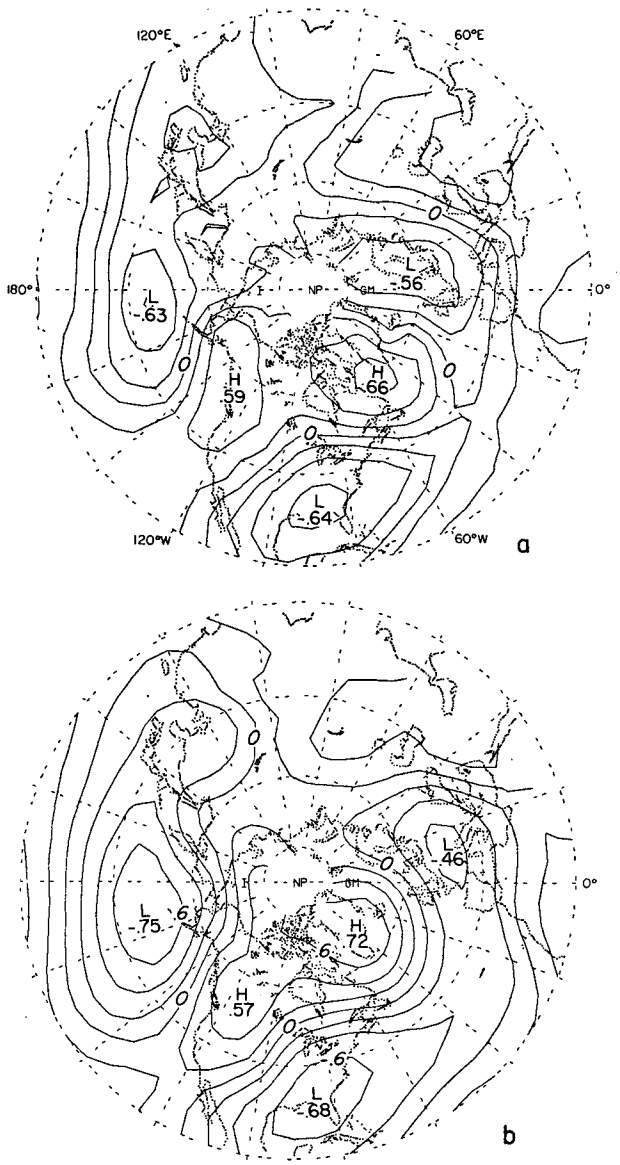

FIG. 3. Sea level pressure at 70°N, 20°W minus sea level pressure at 50°N, 165°W, correlated with (a) 1000–700 mb thickness and (b) 700 mb height. Based on the same 84-month data set as Fig. 2. Contour interval 0.2.

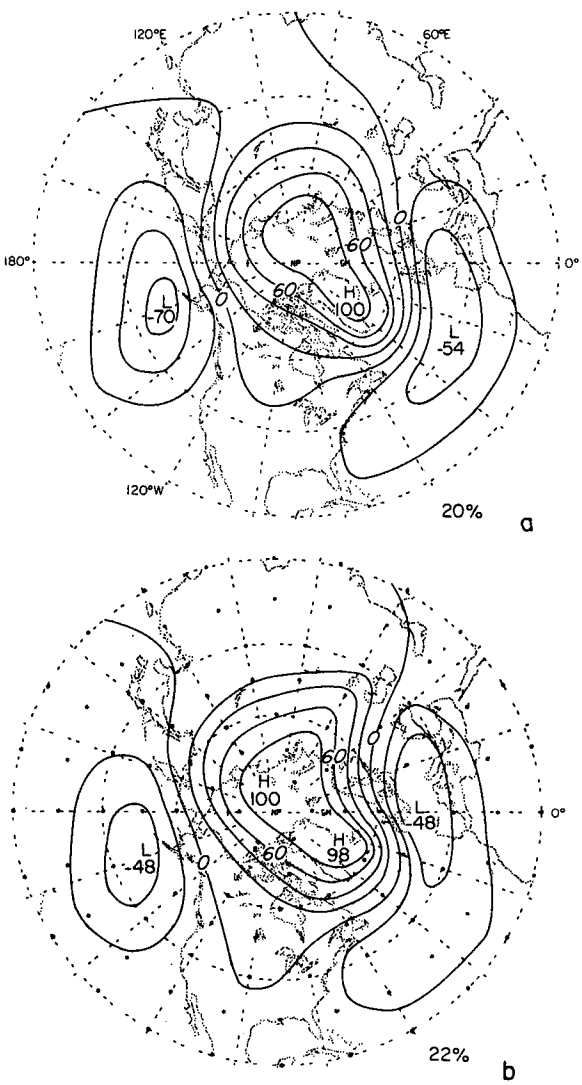

FIG. 4. (a) First mode of an eigenvector analysis expansion of sea level pressure, based on the 66 unnormalized January anomaly fields used by Kutzbach (1970), scaled by setting the largest local value equal to 100. (b) As in (a), but based on the same 84 months data set as Fig. 2. Grid points used in the analysis are marked with dots.

b. The North Pacific Oscillation

Walker and Bliss found evidence of an analogue of the North Atlantic Oscillation in the Pacific

sector with a north-south seesaw in sea level pressure involving a belt in high latitudes extending from eastern Siberia to western Canada and a broad region at lower latitudes including the subtropics and extending poleward to ~40°N. They also described a related thermal pattern with a configuration analogous to the one in the NAO. Because of the sparsity of available data and the marginal level of many of the correlations, their evidence in favor of this so-called North Pacific Oscillation (NPO) was not fully convincing. Rogers (1981) has documented the existence of the NPO on the basis of a more comprehensive data set.

c. The zonally symmetric seesaw

The North Atlantic and North Pacific Oscillations are both characterized by north–south seesaws or standing oscillations in the sea level pressure field with a node located near 50° latitude. In view of the existence of these regional scale patterns, one might expect sea level pressures in polar and temperate latitudes to be negatively correlated. However, the zonally symmetric appearance of the eigenvector patterns in Fig. 4 suggests that such negative correlations might exist even in the absence of the North Atlantic and North Pacific Oscillations. We will show further evidence in Section 5 that the observed negative correlations in zonally averaged sea level pressure anomalies are too strong to be explained on the basis of the contributions from NAO and the NPO. Lorenz (1951) was the first to point out the existence of this zonally symmetric seesaw in the sea level pressure field.

A similar pattern of pressure anomalies has been observed in connection with two stratospheric phenomena: sudden warmings and the quasi-biennial oscillation (QBO). The pressure changes associated with sudden warmings (sharp rises in polar regions and smaller decreases in temperate latitudes) are most clearly evident at stratospheric levels, but in the case of at least one very strong warming event they were accompanied by large sea-level pressure changes in the same sense (see Quiroz, 1977). Ebdon (1975) presented rather provocative observational evidence to the effect that Northern Hemisphere winters in which the phase of the QBO at 50 mb in the tropics is easterly are characterized by higher sea level pressures in the Arctic and lower sea-level pressures at temperate latitudes than winters in which it is westerly. Both these phenomena might contribute to the observed zonally symmetric seesaw in sea level pressure; whether these contributions are important remains to be seen.

d. The Pacific/North American pattern

Synopticians in the United States have long been aware of certain preferred configurations of the mid-tropospheric geopotential height field in the longitudinal sector extending from the mid-Pacific to eastern North America. Episodes of blocking (much above normal geopotential heights) along the west coast of North America tend to be accompanied by strong negative geopotential height anomalies in the mid-Pacific near 45°N and over the southeastern United States. The alternation between this favored blocking pattern and a more zonally oriented (straight west-to-east) mid-tropospheric flow pattern is reflected in the temporal correlation statistics for these three regions. Allen *et al.* (1940)[5] noted the existence of a negative correlation between sea level pressure in the Aleutian low and what they referred to as the Plateau high over the western United States during the colder part of the year which was most pronounced in seasonal mean statistics; somewhat less pronounced in 5-day mean statistics, and only weakly evident in day-to-day fluctuations. Namias (1951) noted a strong positive correlation between wintertime monthly mean 700 mb heights in the North Pacific at (40°N, 150°W) and Cape Hatteras (35°N, 75°W). Klein (1952) noted the tendency for longwave ridges over the western United States to be accompanied by troughs over the eastern United States and vice versa on monthly mean maps. The full Pacific/North American teleconnection pattern appears in Fig. 2 of Dickson and Namias (1976), and in Fig. 22 of Namias (1978) and in a series of 5-day mean composite anomaly charts presented by Martin (1953)[6] and O'Connor (1969).[7] Other manifestations of this pattern are implicit in Figs. 4 and 5 of Klein *et al.* (1960) and in statistics presented in Klein (1965).[8] In order to illustrate the main features of this pattern, we will expand on the results presented in a recent paper by Dickson (1977),[9] which consist of a set of composite anomaly charts based on five winters (1960–61, 1962–63, 1967–68, 1969–70 and 1976–77) which were characterized by below-normal temperatures over the eastern United States and strong ridges in the 700 mb height field extending from the Pacific Northwest of the United States to the Alaska-Canada border.

Fig. 5a shows the 700 mb height anomalies

[5] Allen, R. A., R. Fletcher, J. Holmboe, J. Namias and H. C. Willett, 1940: Report on an experiment on five-day weather forecasting. *Pap. Phys. Oceanogr. Meteor.*, MIT/WHOI, **8**, 94 pp.

[6] D. E. Martin, 1953: Anomalies in the Northern Hemisphere 5-day mean circulation patterns. Air Weather Service Rep. No. 105-100, 39 pp.

[7] J. T. O'Connor, 1969: Hemispheric teleconnections of mean circulation anomalies at 700 mb. ESSA Tech. Rep. WB-10, $$ pp.

[8] W. H. Klein, 1965: Application of synoptic climatology and short-range numerical prediction to five-day forecasting. U.S. Weather Bureau. Res. Pap. No. 46, 79–84.

[9] R. R. Dickson, 1977: Winter 1976–77: A comparison of circulation statistics with other winters. *Proceedings of the Second Annual NOAA Climate Diagnostics Workshop*, pp. 7-1 to 7-12.

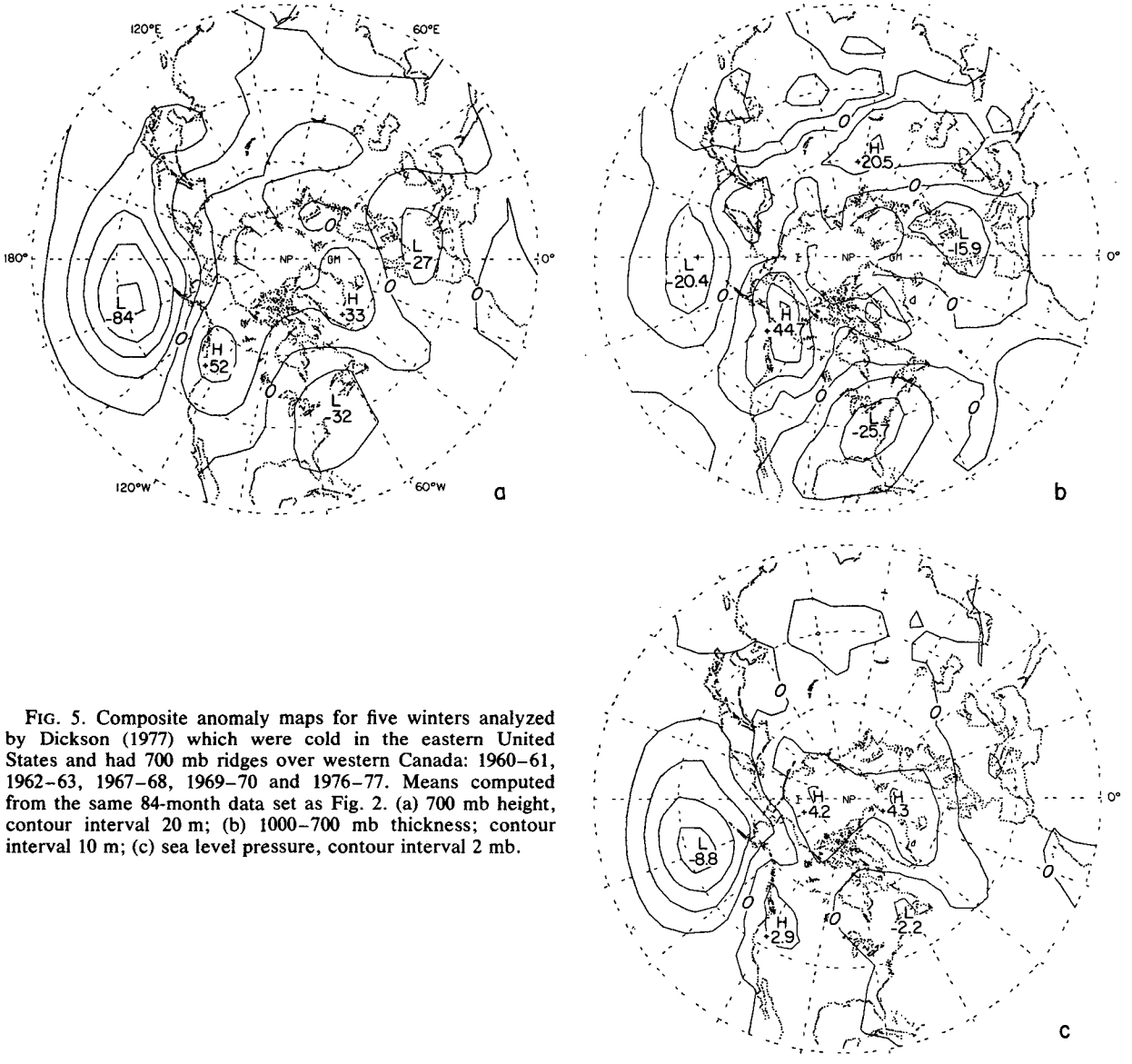

FIG. 5. Composite anomaly maps for five winters analyzed by Dickson (1977) which were cold in the eastern United States and had 700 mb ridges over western Canada: 1960–61, 1962–63, 1967–68, 1969–70 and 1976–77. Means computed from the same 84-month data set as Fig. 2. (a) 700 mb height, contour interval 20 m; (b) 1000–700 mb thickness; contour interval 10 m; (c) sea level pressure, contour interval 2 mb.

derived from the composite. Note the emergence of the Pacific/North American pattern described above. The corresponding 1000–700 mb thickness anomalies shown in Fig. 5b are rather similar except that the positive anomalies over northwest Canada are accentuated relative to those in Fig. 5a and they extend eastward across the Canadian arctic to a secondary center over Baffin Bay. There is also evidence of negative anomalies over northwestern Europe. These secondary features in the thickness pattern, together with the strong negative anomalies over the southeastern United States, are reminiscent of the thermal pattern associated with the North Atlantic Oscillation. The composite sea level pressure anomaly pattern shown in Fig. 5c also bears some relation to its counterpart in the NAO, with evidence of a seesaw between the Icelandic and Aleutian lows. In retrospect, one can see strong signatures of this same Pacific/North American pattern in Fig. 3, which is based on the sea level pressure difference between grid points located near the centers of the Icelandic and Aleutian lows.

Hence the existence of the North Atlantic Oscillation, described by Walker and Bliss and more recently by van Loon and Rogers, and the Pacific/North American pattern, described by Namias and Dickson and collaborators, are well supported by our analysis. These two phenomena appear to share certain features in common: they both exert an influence on winter temperatures over the eastern United States, and they both involve a seesaw between the depths of the Icelandic and Aleutian lows.

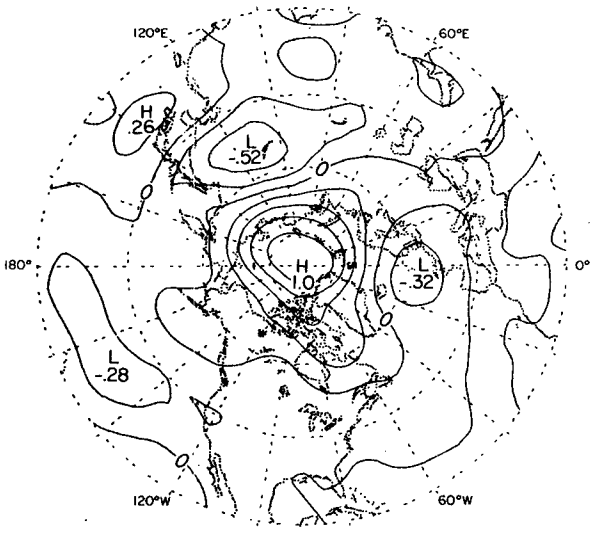

FIG. 6. One-point correlation map showing the correlation coefficient between 500 mb height at the North Pole grid point and 500 mb height every grid point. Based on 45 winter months (Decembers, Januarys and Februarys for the winters 1962–63 to 1976–77). Contour interval is 0.2.

3. Scope of the present study

The conceptual models of teleconnection patterns described in the previous section were first arrived at subjectively by experienced analysts who were concerned about short-term climate variability in specific parts of the hemisphere. In this paper we will consider the teleconnection patterns that emerge from an objective treatment of hemispheric geopotential height data. As a basis for this study, we will make use of monthly mean sea level pressure and 500 mb height data for 45 winter months (Decembers, Januarys, and Februarys for the 15 winters 1962–63 through 1976–77). We will focus our attention on this limited period in order to hold in reserve an independent data set (the winters 1949–50 through 1961–62) for testing the reproducibility of the patterns. We will be interested in determining whether the objectively derived patterns are reproducible, and whether any of them resemble the teleconnection patterns described in the previous section.

4. Analysis techniques

All data used in this study were obtained on magnetic tape from the NCAR data library. Fifteen-year means, computed for each calendar month, were subtracted from the data for individual year-months to obtain anomalies which form the basis for all the correlation statistics described in the paper.

In order to determine, in an objective manner, the nature of any teleconnection patterns which might have existed during the limited time period of our analysis, we began by computing the correlation matrix **R**, whose elements r_{ij} are the temporal correlation coefficients between geopotential height fluctuations at any selected grid point (denoted by the i subscript) and those at every other grid point in the hemisphere (denoted by the j subscript). The columns of **R**, which we will denote as R_i, can be displayed in the form of one-point correlation maps such as the example shown in Fig. 6 for the 500 mb height field, based on the grid point located at the North Pole.

In assessing these correlation maps it is important to have some sense of what constitutes a statistically significant level of correlation. For a sample size of 45 months the 90% *a priori* significance level corresponds to $|r_{ij}| = 0.25$, assuming that each month's anomaly pattern is independent of the others. The effective number of independent samples is clearly somewhat <45; just how much less is difficult to assess because of the problem of deriving stable autocorrelation statistics from such a small data set. A more fundamental problem in assessing the statistical significance of these results is the formulation of appropriate criteria for testing centers of strong correlation which were discovered on an *a posteriori* basis (that is to say, without prior prediction of which elements r_{ij} in R_i would have the largest absolute values). Rather than attempting to specify a formal procedure for testing statistical significance in the face of these difficulties, we will assess statistical significance on the basis of the reproducibility of **R** in an independent data set, the 39 winter months (Decembers, Januarys and Februarys) for the 13 winters beginning with 1949–50 and ending with 1961–62. Results for this independent data set will be shown in Section 7. On the basis of experience, we have found that features with $|r_{ij}| \geq 0.75$ tend to be highly reproducible in the independent data set or in subsets of the original data set. For example, we would not expect the features in Fig. 6 to be highly reproducible except for the positive center surrounding the ith grid point (the North Pole, in this case).

All the one point maps are characterized by a more or less elliptical region of high positive correlation coefficients surrounding the ith or *base grid point*. The size of this bullseye gives an indication of the horizontal scale of the anomalies on the monthly mean maps in the vicinity of the base grid points. On some maps (e.g., the one shown in Fig. 6) this elliptical bullseye is the only feature that appears to be statistically significant; however, in many of the subsequent figures in this paper, the inevitable bullseye surrounding the base grid point is augmented by a secondary feature: a region of rather strong negative correlations which together with the bullseye forms a dipole pattern. Monthly mean geopotential height anomalies tend to be of opposite sign in the vicinity of the two centers of the dipole. There is

a strong tendency for the axes of these dipole patterns to have a north–south orientation, particularly at lower latitudes.

Dipole shaped patterns and more complicated patterns consisting of multiple centers of action on the one-point correlation maps might be indicative of standing oscillations with geographically fixed notes and antinodes, but they could also be caused by propagating wavelike oscillations with preferred zonal and/or meridional scales. For example, Thiebaux (1977) has shown that horizontal structure functions for day-to-day geopotential height fluctuations in middle latitudes exhibit regions of negative correlation centered ~2000 km east and west of the base grid point which are simply a reflection of the tendency for eastward propagating synoptic-scale disturbances to have a preferred range of zonal wavelengths centered ~4000 km.

If the patterns on the one-point correlation maps are truly indicative of standing oscillations with geographically fixed nodes and antinodes, it seems reasonable to expect that grid points located near the antinodes should exhibit much stronger patterns than other points in the hemisphere. On the other hand, if the patterns are indicative of propagating disturbances with preferred scales, strengths and shapes of the teleconnection patterns surrounding each grid point in a given latitude belt should be rather similar.

A simple method of contrasting the strengths of teleconnection patterns for different grid points is to compare the strongest negative correlation on their respective one-point correlation maps. To facilitate such a comparison we have plotted in Fig. 7 at the location of the base grid point the strongest negative correlation on each of the one-point correlation maps. For example, on the teleconnection map for the North Pole, shown in Fig. 6, the strongest negative correlation is −0.52 which occurs at the grid point (50°N, 115°E); this value is assigned to the North Pole grid point in Fig. 7b. Formally, Fig. 7 is derived directly from the correlation matrix **R** by mapping the row vector **T** whose elements T_i are the minimum (strongest negative) values of r_{ij} in the ith column of **R**, i.e.,

$$T_i = \left|(r_{ij}) \text{ minimum for all } j\right|.$$

The minus signs are omitted for the sake of convenience and T_i is termed the teleconnectivity of the ith grid point.

The resulting patterns in Fig. 7 show strong regional variations in teleconnectivity, which attest to the reality of standing wave oscillations with geographically distinct nodes and antinodes. Note that values of the teleconnectivity tend to be larger at the 500 mb level (Fig. 7b) than at the 1000 mb level (Fig. 7a).

It is possible to display additional information

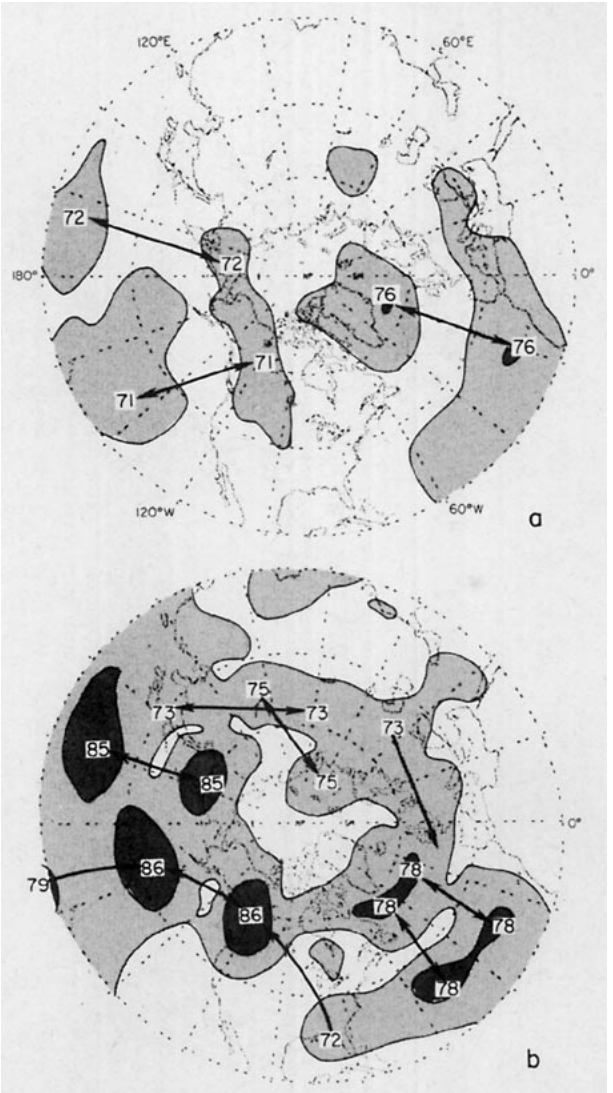

FIG. 7. Strongest negative correlation ρ_i on each one-point correlation map, plotted at the base grid point (referred to in text as "teleconnectivity") for (a) sea-level pressure and (b) 500 mb height. Based on 45 winter months (Decembers, Januarys, and Februarys for winters 1962–63 through 1976–77). Negative signs have been omitted and correlation coefficients multipled by 100. Regions where $\rho_i < 60$ are unshaded; $60 \leq \rho_i < 75$ stippled lightly; $75 \leq \rho_i$ stippled heavily. Arrows connect centers of strongest teleconnectivity with the grid point which exhibits strongest negative correlation on their respective one-point correlation maps.

concerning the structure of the correlation matrix **R** on the teleconnectivity maps by drawing arrows from the various centers of strong teleconnectivity to the grid points with which they show the strongest negative correlation on their respective one-point correlation maps. In the case of simple, dipole-shaped teleconnection patterns, the arrows go in both directions, because of the symmetry of **R**.

Fig. 7a provides an objective confirmation of the sea level pressure pattern associated with the North

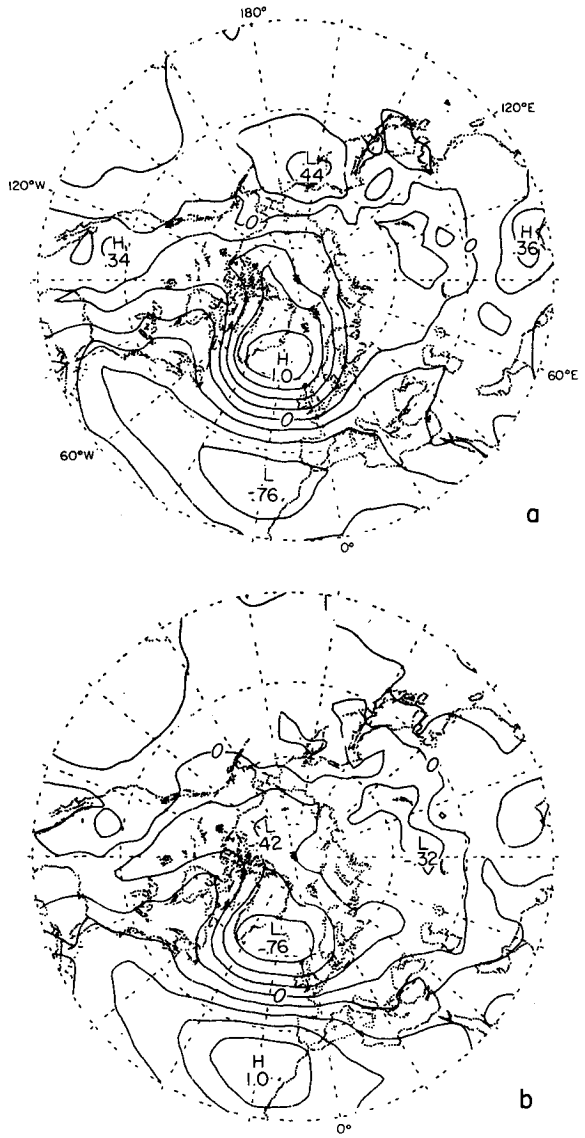

FIG. 8. One-point correlation maps showing correlation coefficient between sea-level pressure at the grid points (a) 65°N, 20°W and (b) 30°N, 20°W, and sea-level pressure at every grid point. Based on same 45-month data set as Fig. 7a. Contour interval is 0.2.

Atlantic Oscillation; the seesaw between the region near Iceland and lower latitudes of the Atlantic Ocean comes through as the strongest negative correlation in **R**. The negative correlations between the subtropical Pacific and Eastern Siberia and Alaska may be regarded as a confirmation of the North Pacific Oscillation sea level pressure pattern described by Walker and Bliss (1932). The dipole pattern located further east in the Pacific is in the proper position to be a reflection of the Pacific/North American pattern described in Section 2. All the strong negative correlations in this figure involve seesaws between sea level pressure in the lobe-shaped region at high latitudes and regions in the subtropical oceanic anticyclones.

The teleconnections at the 500 mb level (Fig. 7b) tend to be stronger than those at 1000 mb and somewhat more complex. There is strong confirmation of the Pacific/North American pattern and evidence of a strong north–south seesaw in the Atlantic sector which is probably associated with the North Atlantic Oscillation. There is also evidence of a strong dipole pattern over the western Pacific, and east–west teleconnections over the Eurasian land mass.

In the next two sections we will examine, by means of a number of different analysis approaches, the primary teleconnection patterns displayed in Fig. 7. We will also determine whether similar patterns appear among the leading eigenvectors of the correlation matrix **R**.

5. Sea level pressure teleconnection patterns

a. The North Atlantic and North Pacific patterns

We now consider in more detail the strong dipole pattern in the North Atlantic as revealed by Fig. 7a. Fig. 8 shows one-point correlation maps for the two centers of maximum teleconnectivity, the grid points (65°N, 20°W) and (30°N, 20°W), based on the 15 winter data set 1962–63 to 1976–77. These patterns obviously bear the signature of the North Atlantic Oscillation. Therefore, it is of interest to compare Fig. 8 with Fig. 2 of this paper and Fig. 11 of van Loon and Rogers (1978), both of which were constructed making use of an index of the NAO: the Jakobshavn-Oslo temperature difference. Our Fig. 2, in which sea level pressure at each grid point is correlated directly with the index shows the same major features as Fig. 8. The most important difference between the patterns is the northeastward shift of the low-latitude center of action toward the Mediterranean Sea in Fig. 2, relative to Fig. 8. Fig. 11 of van Loon and Rogers is analogous to our Fig. 8a except that it is based on data for 53 seesaw winters which were characterized by large absolute values of the index (Greenland warm with Scandinavia cold; or Greenland cold with Scandinavia warm). The resulting pattern shows a strong similarity to Fig. 8a in the Atlantic sector, but it includes an additional center of action near (36°N, 160°W) which is not reproduced well in our Fig. 8. Apparently, this Pacific center shows a strong negative correlation with sea-level pressure in the vicinity of the Icelandic low only during the seesaw winters, whereas the north–south correlations in the Atlantic sector are observed during all winters.

In Fig. 9, 1000–500 mb thickness and 500 mb height over the hemisphere are correlated with the sea level pressure difference between the two centers in Fig. 8. The thickness plot (Fig. 9a) shows a clear signature of the temperature seesaw between

Greenland and Scandinavia documented by van Loon and Rogers (1978), including the secondary features over the eastern United States and the Middle East. The similarity of the 500 mb correlation map in Fig. 9b to the pattern in Fig. 8 demonstrates the tendency for strong vertical coupling of the geopotential height field over the midlatitude oceans. [Blackmon *et al.* (1979) found positive correlations between simultaneous wintertime monthly mean sea level pressure and 500 mb height as high as 0.95 in the North Atlantic.] The 500 mb features are shifted westward slightly relative to those in the sea level pressure field, and they have a somewhat more wavelike appearance in the longitude domain.

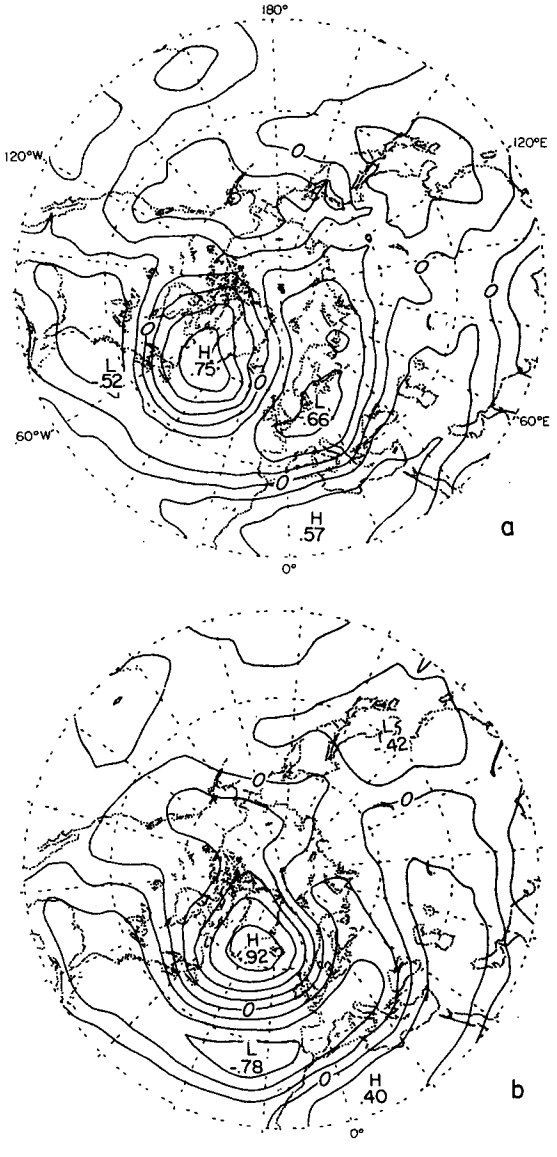

FIG. 9. Correlation coefficient between sea level pressure at (65°N, 20°W) minus sea-level pressure at (30°N, 20°W) and (a) 100–500 mb thickness and (b) 500 mb height. Based on the same 45-month data set as Fig. 7a. Contour interval is 0.2.

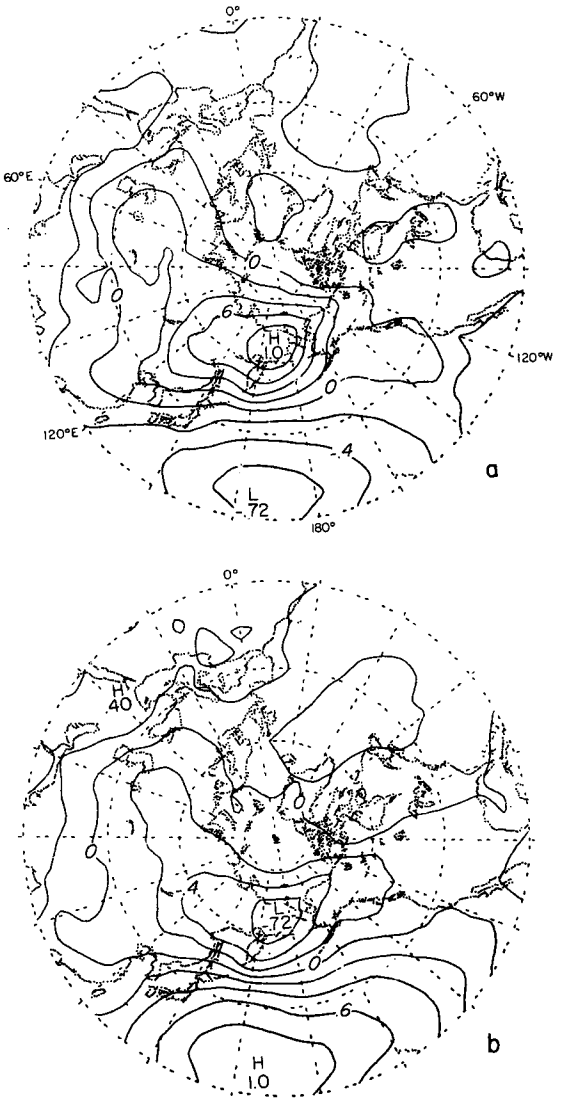

FIG. 10. As in Fig. 8, but for base grid points (a) 65°N, 170°E and (b) 25°N, 165°E.

A slightly weaker teleconnection pattern with a similar structure is located in the western Pacific Ocean, with centers located at (65°N, 170°E) and (25°N, 165°E). One-point correlation maps for these grid points are shown in Fig. 10. This pattern is clearly analogous to the North Pacific Oscillation described by Walker and Bliss (1932) and Rogers (1981). It is also closely related to one of the major teleconnection patterns in the 500 mb height field, our "Western Pacific" pattern described in Section 6d.

b. Results of eigenvector analysis

Fig. 11 shows the structure of the first eigenvector (or empirical orthogonal function) of the (a) covariance matrix and (b) the normalized covariance matrix **R** of the sea level pressure field, as repre-

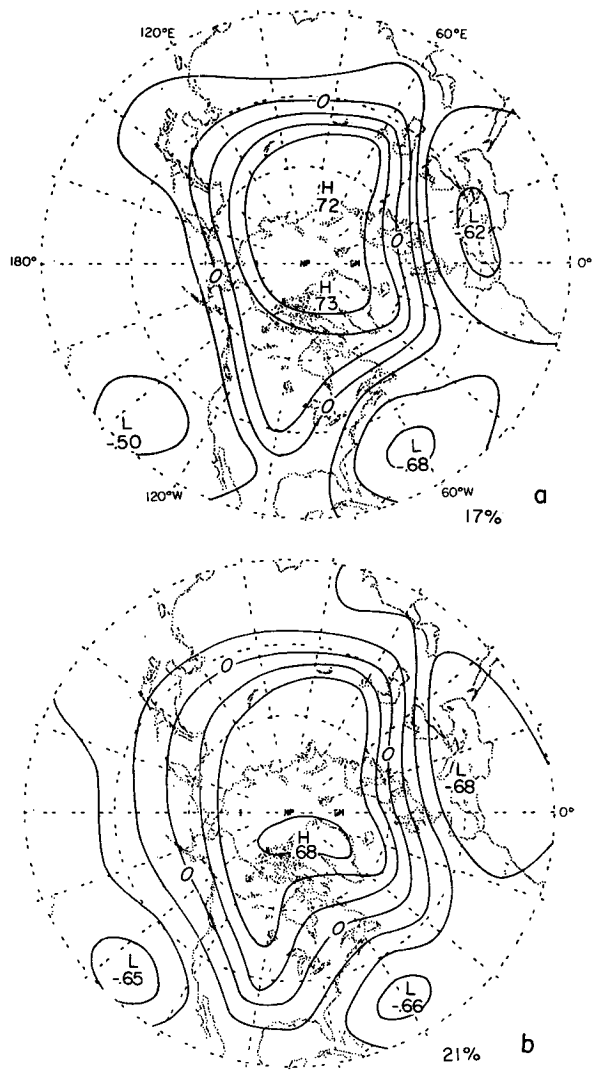

FIG. 11. Horizontal structure of the first mode of an eigenvector analysis expansion of sea level pressure, as computed from (a) the covariance matrix, and (b) the normalized covariance matrix. Based on the same 45-month data set as Fig. 7a. Amplitudes are scaled so as to show the value of the (temporal) correlation coefficient between the coefficient of the first eigenvector and the monthly mean geopotential height anomalies at each grid point. The sign convention is arbitrary. Contour interval is 0.2.

sented by the grid points denoted by dots in Fig. 4b. The fields displayed in Fig. 11 are correlation coefficients $r(p_j, c_k)$, where p_j is the time series of sea level pressure at the jth grid point and c_k is the time series of the coefficients of the kth (in this case, the first) eigenvector.[10] Both patterns displayed in Fig. 11 are characterized by negative correlations between sea level pressure fluctuations in polar regions and those at latitudes equatorward of 50°N, in general agreement with the teleconnectivity pattern in Fig. 7a. For this particular 15-winter data set, the North Atlantic Oscillation shows up even less distinctly than in the 28-winter data set analyzed in Fig. 4b. The second eigenvector (not shown) is dominated by a zonal wavenumber 1 pattern which bears little relation to any of the teleconnection patterns described in this paper.

[10] In the case of the results for the normalized covariance matrix, the desired correlation coefficients are the eigenvector components e_{jk} scaled such that $\sum_j (e_{jk})^2 = \lambda_k$, where λ_k is the kth eigenvalue.

c. *Discussion*

The analyses described in the previous two subsections emphasize different aspects of the structure of the correlation matrix **R** of the sea level pressure field: the patterns revealed by the teleconnectivity map and elaborated on in Figs. 8 and 10 are essentially regional in scale, whereas the leading eigenvector of the correlation matrix is dominated by a planetary scale, zonally symmetric seesaw between sea level pressures in the polar cap region and lower latitudes. Analyses based on correlations between stations lying more or less along the same latitude circle, such as that of van Loon and Rogers (1978), inevitably tend to emphasize the regional scale patterns, whereas analyses based on north–south correlations pick up more of the planetary-scale pattern. The latter pattern can be clearly seen in the correlation matrix of zonally averaged sea level pressure, shown in Table 1. The negative correlations between subtropical latitudes and the region poleward of 50°N are as strong as the strongest local negative correlations in Fig. 7a.

6. 500 mb teleconnections

The 500 mb height field, when analyzed in the same manner as the sea-level pressure field, is characterized by a more complex network of teleconnection patterns, as was shown in Fig. 7. Examination of the one-point correlation maps which make up Fig. 7 reveals five patterns: two are spread over the eastern oceans and western continents (we have named these the eastern Atlantic and Pacific/North American patterns), two are meridionally oriented "dipoles" in the western oceans (the western Atlantic and western Pacific patterns) and one extends eastward from Scandinavia to Korea (the Eurasian pattern).

a. *The eastern Atlantic pattern*

The eastern Atlantic pattern is characterized by three centers: one located southwest of the Canary Islands (25°N, 25°W), another west of Great Britain (55°N, 20°W), and a third near the Black Sea (50°N, 40°E). The one-point correlation maps for these grid points are presented in Fig. 12.

TABLE 1. Correlation between zonally averaged sea level pressures at various latitudes, based on the same 45-month data set as Fig. 7a.

	20°	25°	30°	35°	40°	45°	50°	55°	60°	65°	70°
75°	−0.58	−0.59	−0.54	−0.55	−0.57	−0.47	−0.13	0.28	0.63	0.84	0.96
70°	−0.68	−0.67	−0.61	−0.59	−0.57	−0.40	0.01	0.46	0.79	0.95	
65°	−0.76	−0.76	−0.69	−0.64	−0.55	−0.28	0.21	0.68	0.93		
60°	−0.80	−0.80	−0.74	−0.65	−0.48	−0.10	0.45	0.88			
55°	−0.72	−0.69	−0.59	−0.43	−0.16	0.30	0.80				
50°	−0.44	−0.34	−0.17	0.08	0.40	0.79					
45°	0.03	0.19	0.38	0.62	0.86						
40°	0.42	0.60	0.77	0.92							
35°	0.66	0.82	0.95								
30°	0.83	0.95									
25°	0.95										

Sawyer (1970, Fig. 12) presented a 500 mb one-point correlation map for (55°N, 20°W) using time-filtered daily data for a 3-year period. The filter emphasized fluctuations in the period range from 15 to 60 days. Although the pattern he obtained was very similar in shape to the one in Fig. 12b, the strongest correlations at points distant from the central bullseye were smaller in magnitude than those

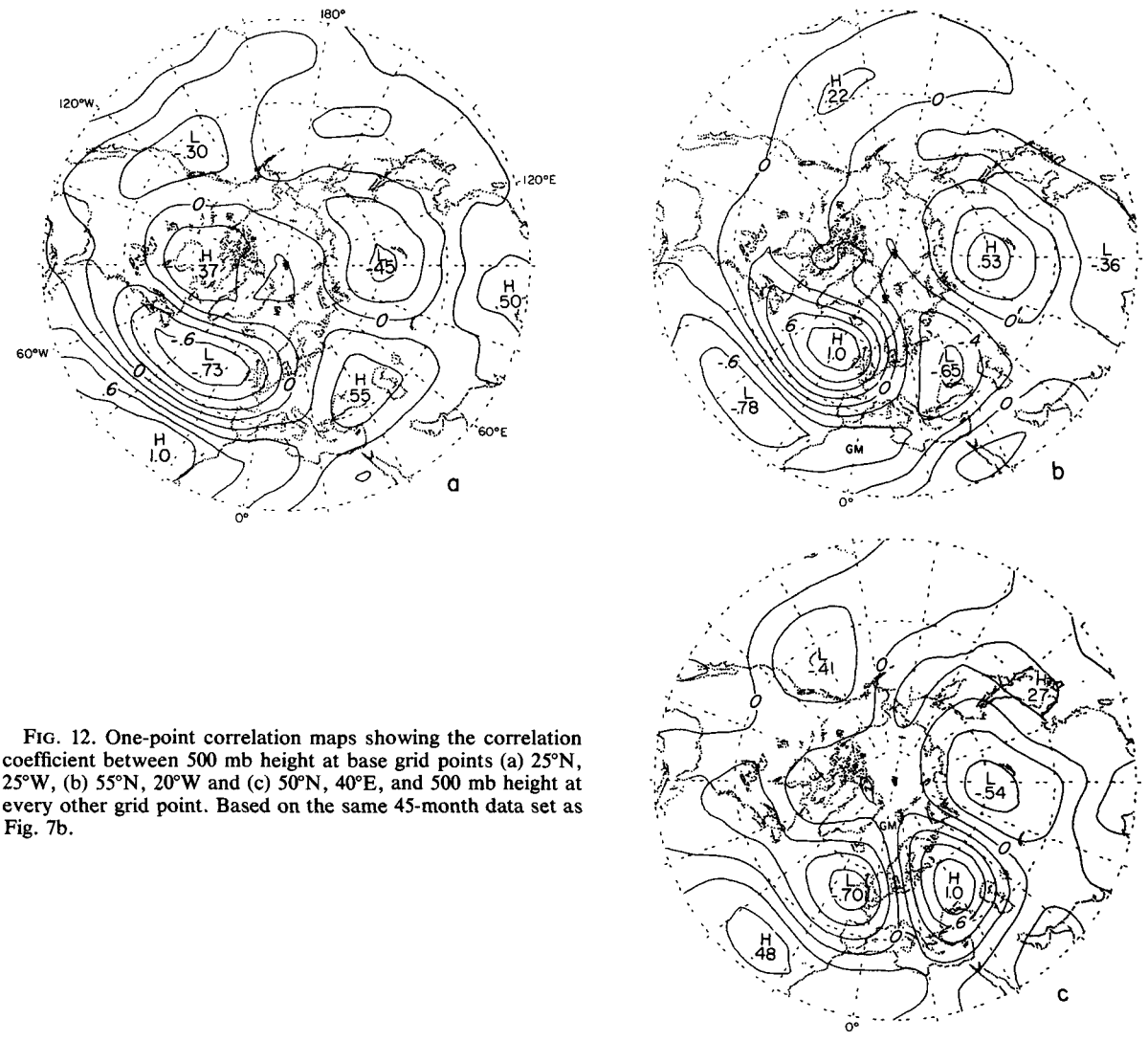

FIG. 12. One-point correlation maps showing the correlation coefficient between 500 mb height at base grid points (a) 25°N, 25°W, (b) 55°N, 20°W and (c) 50°N, 40°E, and 500 mb height at every other grid point. Based on the same 45-month data set as Fig. 7b.

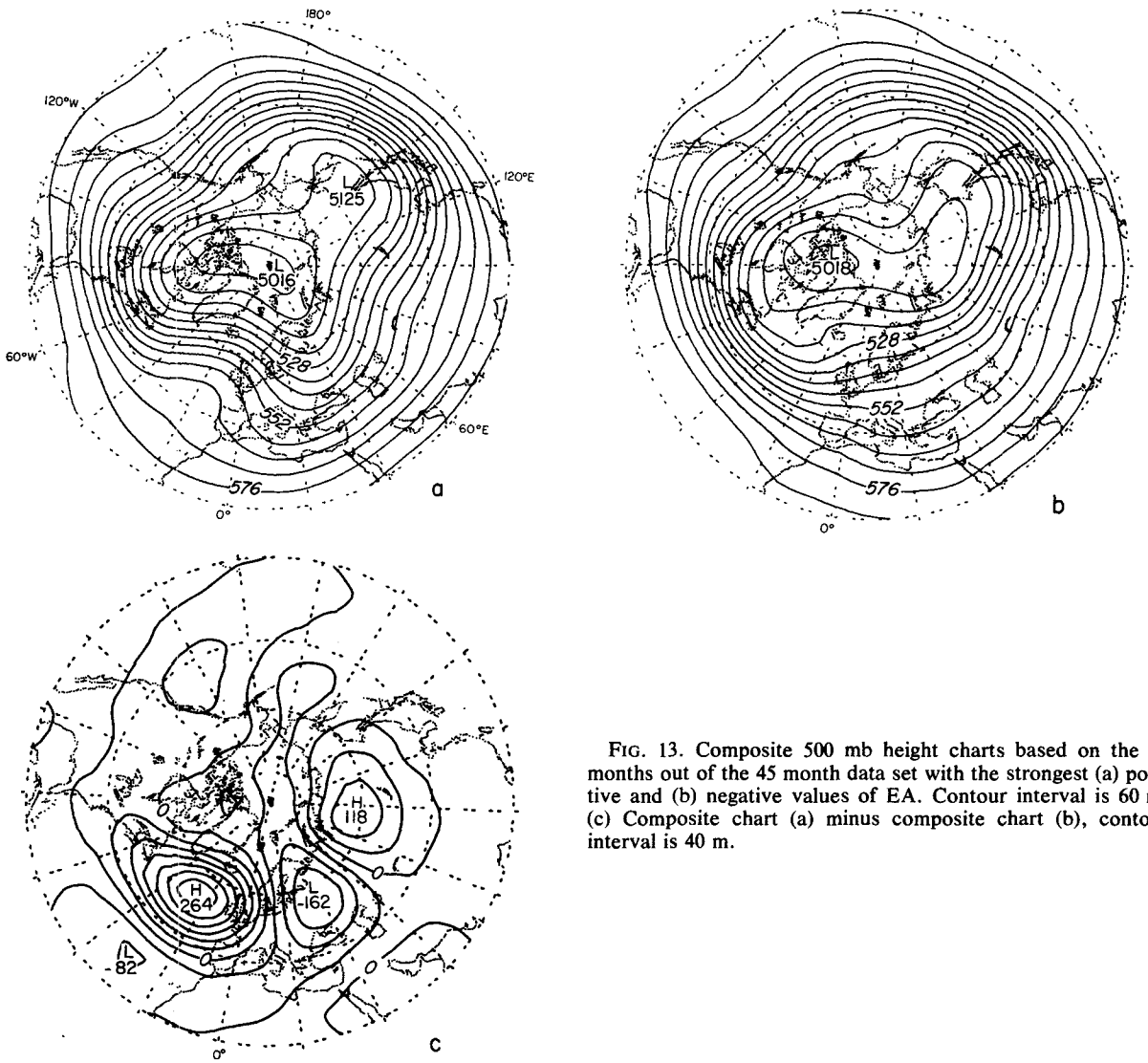

FIG. 13. Composite 500 mb height charts based on the 10 months out of the 45 month data set with the strongest (a) positive and (b) negative values of EA. Contour interval is 60 m. (c) Composite chart (a) minus composite chart (b), contour interval is 40 m.

reported here. This difference may be due to the fact that the patterns appear more distinctly in the wintertime data (upon which our study is based) than in the data for other seasons (which were included in Sawyer's analysis).

For purposes of compositing, we will define a monthly mean pattern index based on normalized 500 mb height anomalies (denoted by the symbol z^*)[11] at specified grid points corresponding to "centers of action" or antinodes of the pattern. The eastern Atlantic pattern index is defined as

$$EA = \tfrac{1}{2}z^*(55°N, 20°W) - \tfrac{1}{4}z^*(25°N, 25°W) - \tfrac{1}{4}z^*(50°N, 40°E).$$

Thus, a positive pattern index is indicative of anomalously high 500 mb height over the North Atlantic and low heights over the subtropical Atlantic and eastern Europe; a negative pattern index indicates anomalies in the opposite sense. In order to make the sum of the weights equal to zero in EA, the first grid point (55°N, 20°W) has somewhat arbitrarily been assigned twice the weight of the other two grid points.

Figs. 13a and 14a are 500 mb height and sea level pressure composites, respectively, based on 10 months (of the 45 winter months included in the 15 winter record) with the strongest positive pattern indices. Figs. 13b and 14b are the corresponding composites for the 10 months when EA was most negative. (The complete time series of indices for all five patterns described in this section is presented in Table 3 of Section 6f). The individual monthly maps included in these composites were adjusted by

[11] Normalized anomalies are based on local 15-year means and standard deviations for each respective calendar month.

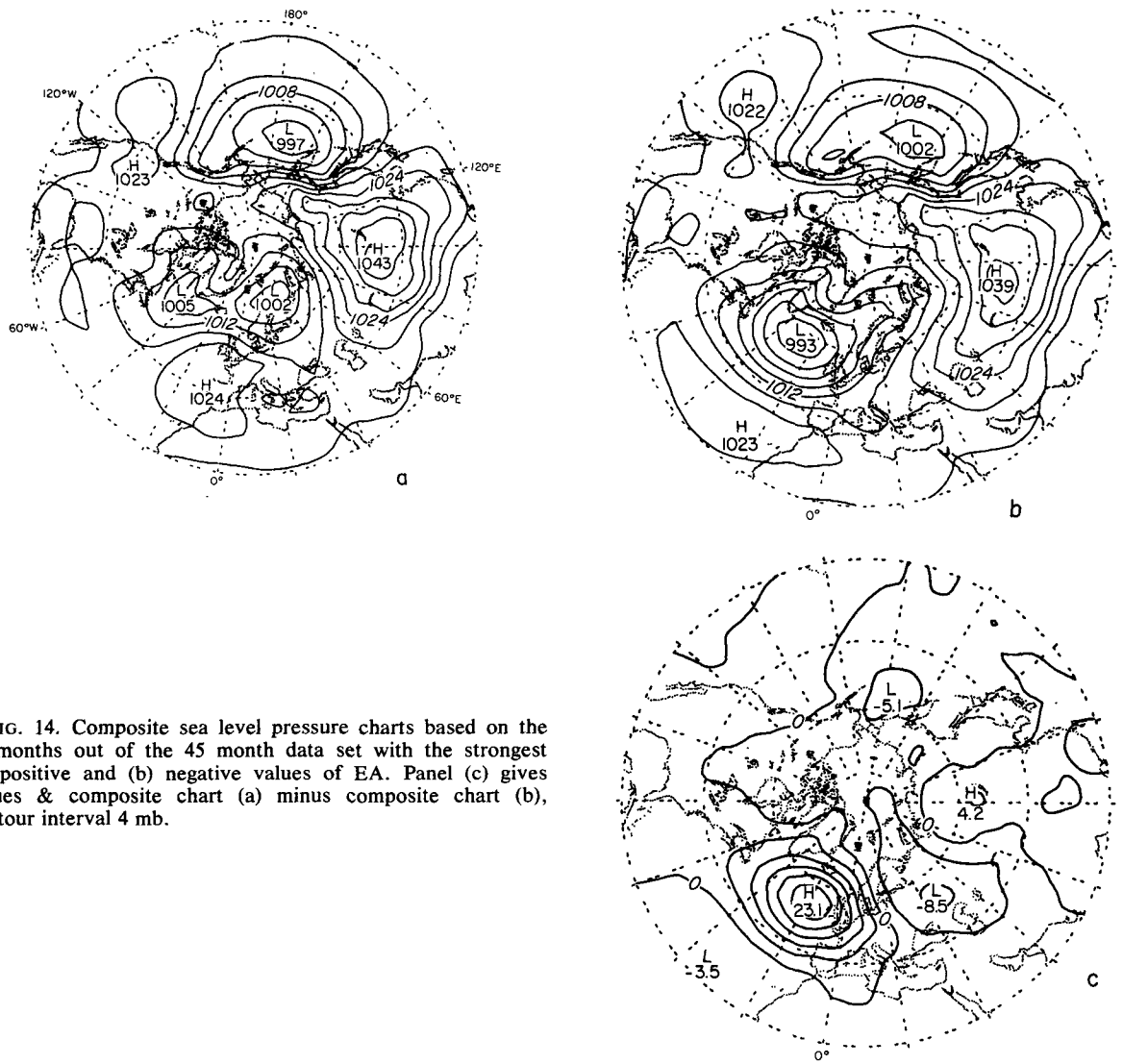

FIG. 14. Composite sea level pressure charts based on the 10 months out of the 45 month data set with the strongest (a) positive and (b) negative values of EA. Panel (c) gives values & composite chart (a) minus composite chart (b), contour interval 4 mb.

subtracting from the value at each grid point the difference between the mean for the calendar-month and the mean for the 3-month winter season. This small adjustment was performed in order to make the results independent of the distribution of calendar months which happen to be included in any particular composite. Composite maps computed with and without this adjustment turned out to be virtually identical.

The 500 mb composite for EA positive (Fig. 13a) shows a strong ridge off the European coast together with a trough extending from the Barents Sea southward and westward into the Mediterranean. The contrasting months (Fig. 13b) are characterized by a much more zonal flow over the eastern Atlantic and western Europe. Features over eastern Asia and the Pacific Ocean in both composites resemble those found on a winter mean map (not shown); 500 mb height in these regions is almost completely uncorrelated with the eastern Atlantic pattern index. Fig. 13b was subtracted from Fig. 13a to produce the difference composite shown in Fig. 13c, which therefore represents the 500 mb height difference between the two extremes of the eastern Atlantic pattern. Features seen in Fig. 13c are qualitatively similar to those found on the correlation maps in Fig. 12. However, the difference map reflects the geographical distribution of the temporal variance of 500 mb height. Pattern centers located near maxima in the 500 mb height variance field (see Blackmon *et al.* (1979), Fig. 1b) tend to show larger differences in these composite maps than centers located in regions of lower variance. The contrast in amplitude is particularly sharp between northern and subtropical regions over the oceans; in Fig. 13c, the 500 mb height differences near the British center are over three times as large as those near the center of action in the subtropical Atlantic. The British

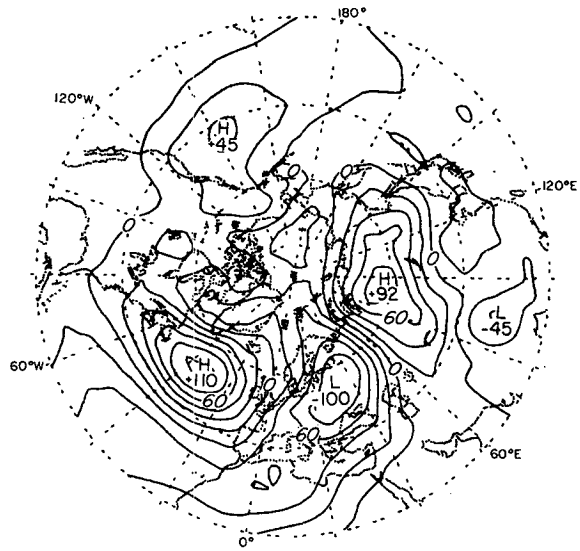

FIG. 15. 1000–500 mb thickness difference chart formed from the composite chart for the 10 months out of the 45-month data set with the strongest positive values of EA minus the 10 months with the strongest negative values. Contour interval is 20 m, which corresponds to a 1 K difference in the mean virtual temperature of the layer.

Center shows the most dramatic differences in the composites not only because of its higher variance, but also because its 500 mb height is more strongly correlated with EA than are the 500 mb heights at the other two centers of action.

Inspection of the corresponding three charts for sea level pressure shown in Fig. 14, reveals that during EA positive months the Icelandic low is reduced in strength and split into two centers, while the Atlantic subtropical high is displaced far to the north of its normal climatological position. EA negative months are characterized by an intense Icelandic low with a broad, strong high directly to the south. The composite difference map is dominated by a single strong center of action located to the west of the British Isles. The sea level pressure composites also show a negative correlation between the strength of the Icelandic and Aleutian lows.

Composite maps of 1000–500 mb thickness also were computed using data for the same sets of months. The thickness difference map, shown in Fig. 15, gives an indication of the lower tropospheric temperature difference between the two extremes of the eastern Atlantic pattern. The strongest thickness contrasts are closely associated with the centers of action in the 500 mb height field shown in Fig. 12. Hence, to a first approximation, this anomaly pattern exhibits an equivalent barotropic structure, with amplitude increasing with height and only a weak westward tilt with increasing height. The westward tilt with height is most apparent in the westward displacement of the major features in the thickness field relative to those in the sea level pressure field. The Greenland-Scandinavia temperature seesaw studied by van Loon and Rogers (1978) is evidently not associated with this pattern, since the same thickness difference contour (−20 m) intersects southern Greenland and southern Norway in Fig. 15.

b. The Pacific/North American pattern

The Pacific/North American pattern is comprised of four centers; one is located near Hawaii (20°N, 160°W), a second over the North Pacific Ocean (45°N, 165°W), a third over Alberta (55°N, 115°W), and a fourth over the Gulf Coast region of the United States (30°N, 85°W). One-point correlation maps for these centers are shown in Fig. 16. The position of this pattern with respect to the Pacific Ocean and North American continent is somewhat analogous to the situation of the eastern Atlantic pattern over the Atlantic Ocean and Europe. The pattern seen in each map in Fig. 16 is essentially identical to the one identified by Namias and collaborators and described in Section 2c of this paper.

The Pacific/North American pattern index for each winter month is defined as a linear combination of the normalized height anomalies at the four pattern centers:

$$\mathrm{PNA} = \tfrac{1}{4}[z^*\,(20°\mathrm{N}, 160°\mathrm{W}) - z^*\,(45°\mathrm{N}, 165°\mathrm{W}) + z^*\,(55°\mathrm{N}, 115°\mathrm{W}) - z^*\,(30°\mathrm{N}, 85°\mathrm{W})].$$

Thus, the sign of PNA will be positive during months with strong ridges over western Canada.

Figs. 17–19 are composite maps based on winter months with the 10 highest and 10 lowest values of PNA. Positive values of PNA (Fig. 17a) are associated with the amplified wave pattern reminiscent of several recent winters and the winters included in Dickson's composite (Fig. 5), while negative values (Fig. 17b) correspond to a more zonally oriented 500 mb height field. The difference map (Fig. 17c) resembles the one in Dickson's composite (Fig. 5a).

Sea level pressure composites are shown in Fig. 18. Positive values of PNA are characterized by a deep Aleutian low, situated in the region of negative 500 mb height anomalies. Conversely, the Aleutian low is anomalously weak during negative PNA months. An inverse relationship between the depth of the Aleutian and Icelandic lows is also evident in these composites. The difference pattern (Fig. 18c) is dominated by the anomalies in the North Pacific, as in Dickson's composite (Fig. 5c).

The difference between the 1000–500 mb thickness composites derived from Figs. 17 and 18 is presented in Fig. 19. Again, the pattern is indicative of a cold core equivalent barotropic structure with a correspondence between positive height anomalies and positive thickness anomalies (warm ridges and

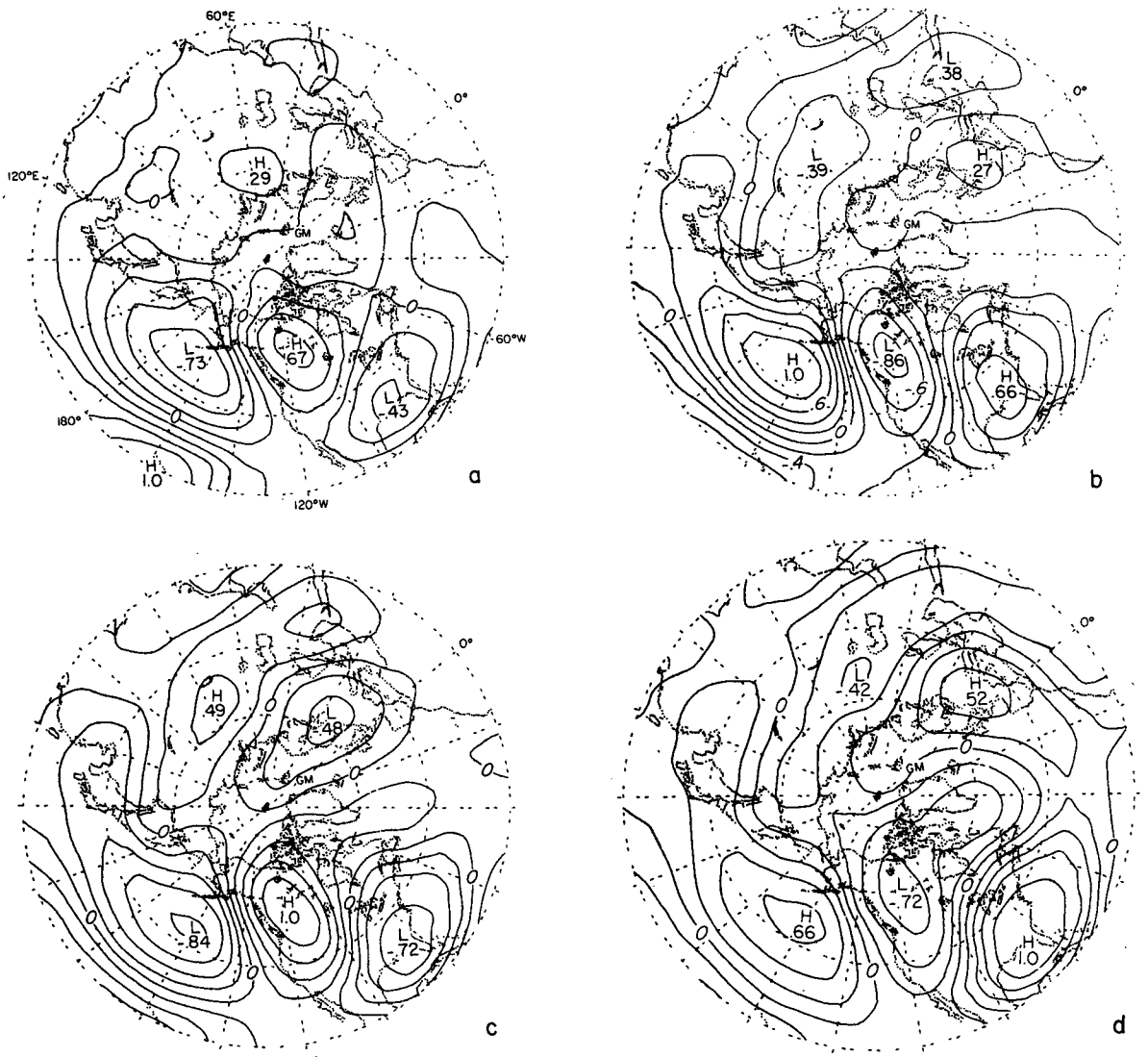

FIG. 16. As in Fig. 12, but for base grid points (a) 20°N, 160°W; (b) 45°N, 165°W; (c) 55°N, 115°W; (d) 30°N, 85°W.

cold troughs). As in Fig. 5, the thickness anomalies over Greenland and northwestern Europe are somewhat more pronounced than the corresponding anomalies in the 500 mb height pattern, and the overall pattern shows a rather remarkable resemblance to the pattern in Fig. 3a, which was derived on the basis of an entirely different compositing scheme suggested by van Loon and Rogers' (1978) analysis of the North Atlantic Oscillation.

Table 2 documents the relationships between the normalized 500 mb height anomalies at the four centers of action in the Pacific/North American pattern for each of the 45 individual months of the 15-winter sample. Boldface plus signs refer to positive anomalies which would be large enough to lie in the upper quintile of the frequency distributions of the individual grid points if these distributions were normal ($z^* \geq 0.84$), ordinary plus signs refer to positive values in the second quintile ($0.84 \geq z^* \geq 0.25$), zeroes to values in the third quintile ($0.25 > z^* \geq -0.25$), and so on. The signs of the anomalies for the North Pacific and Gulf Coast grid points have been reversed, so that months with positive anomalies in the Table at all four grid points are indicative of large positive values of the pattern index and vice versa. Hence, months with anomalies of like sign in Table 1 contribute to the correlation patterns shown in Fig. 16 and months with anomalies of mixed sign detract from the correlations. Note the predominance of positive signs in the winters which are included in Dickson's composite (Fig. 5) based on ridging along the west coast and below-normal temperatures in the eastern United States. The persistence of these anomalies from month to

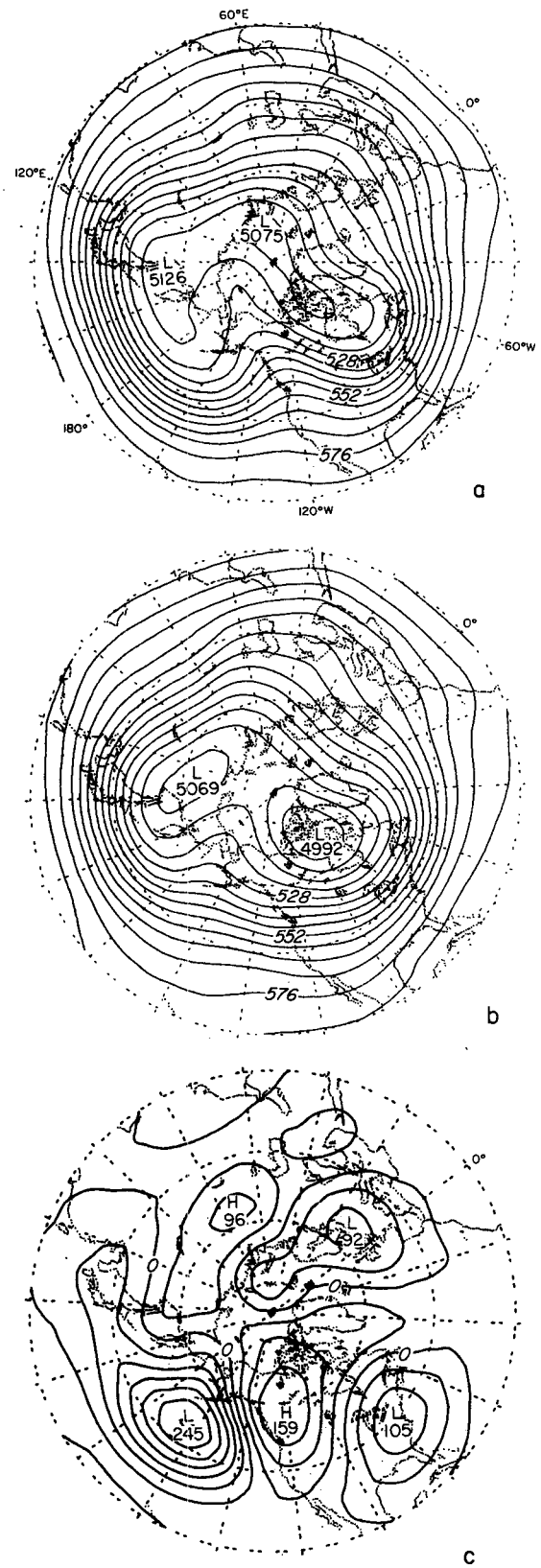

FIG. 17. As in Fig. 13 except for the Pacific/ North American pattern.

month is quite striking. Note also the predominance of negative signs during the winters of 1970–71 and 1971–72, which were characterized by strong zonal flows over the eastern Pacific and western North America.

c. *The western Atlantic pattern*

The teleconnectivity distribution in Fig. 7b suggests the existence of strong teleconnection patterns over the western oceans, anchored in the axes of mean troughs in the 500 mb height field. Both patterns consist of meridionally oriented dipoles, similar in structure to the patterns found over the central oceans in the sea level pressure field. Over the Atlantic Ocean, pattern centers are located at (55°N, 55°W) and (30°N, 55°W). The one-point correlation map for the northern center, shown in Fig. 20a, exhibits two secondary regions of high correlation in addition to the two pattern centers: one located over central Europe and the other over Manchuria. These regions are centers of action of the Eurasian pattern described in Section 6e. For the purposes of compositing, we will define the Western Atlantic pattern index using only the two primary centers of action:

$$WA = \tfrac{1}{2}[z^*\ (55°N, 55°W) - z^*\ (30°N, 55°W)].$$

Composites of months when the western Atlantic (WA) pattern is strong are presented in Figs. 21–23. Positive values of WA correspond to a weak jet stream over the western Atlantic, a weak Icelandic low, and a weak subtropical high in the sea level pressure field and *vice versa*. The differences between the high and low WA composites represent almost a factor of 2 difference in the strength of the Atlantic jetstream and a 17 mb sea level pressure difference near the southern tip of Greenland. The difference pattern in sea level pressure (Fig. 22c) is reminiscent of the strongest teleconnection pattern in the sea-level pressure field (Fig. 8) but the centers of the pattern are displaced ~20° of longitude further to the west. The thickness difference pattern (Fig. 23) resembles the thermal pattern associated with the North Atlantic Oscillation. There is much less of a westward shift of the thickness pattern relative to the sea level pressure pattern than indicated by the idealized model of the NAO in Fig. 1, or in the climatological mean temperature and sea-level pressure fields. Thus, to a first approximation, the western Atlantic pattern is characterized by an equivalent barotropic vertical structure, like the patterns considered previously in this section.

In addition to the features pointed out in the previous paragraph, the western Atlantic pattern exerts an influence upon the circulation over the Eurasian sector of the hemisphere. We will consider these aspects of the pattern in more detail in Section 6e.

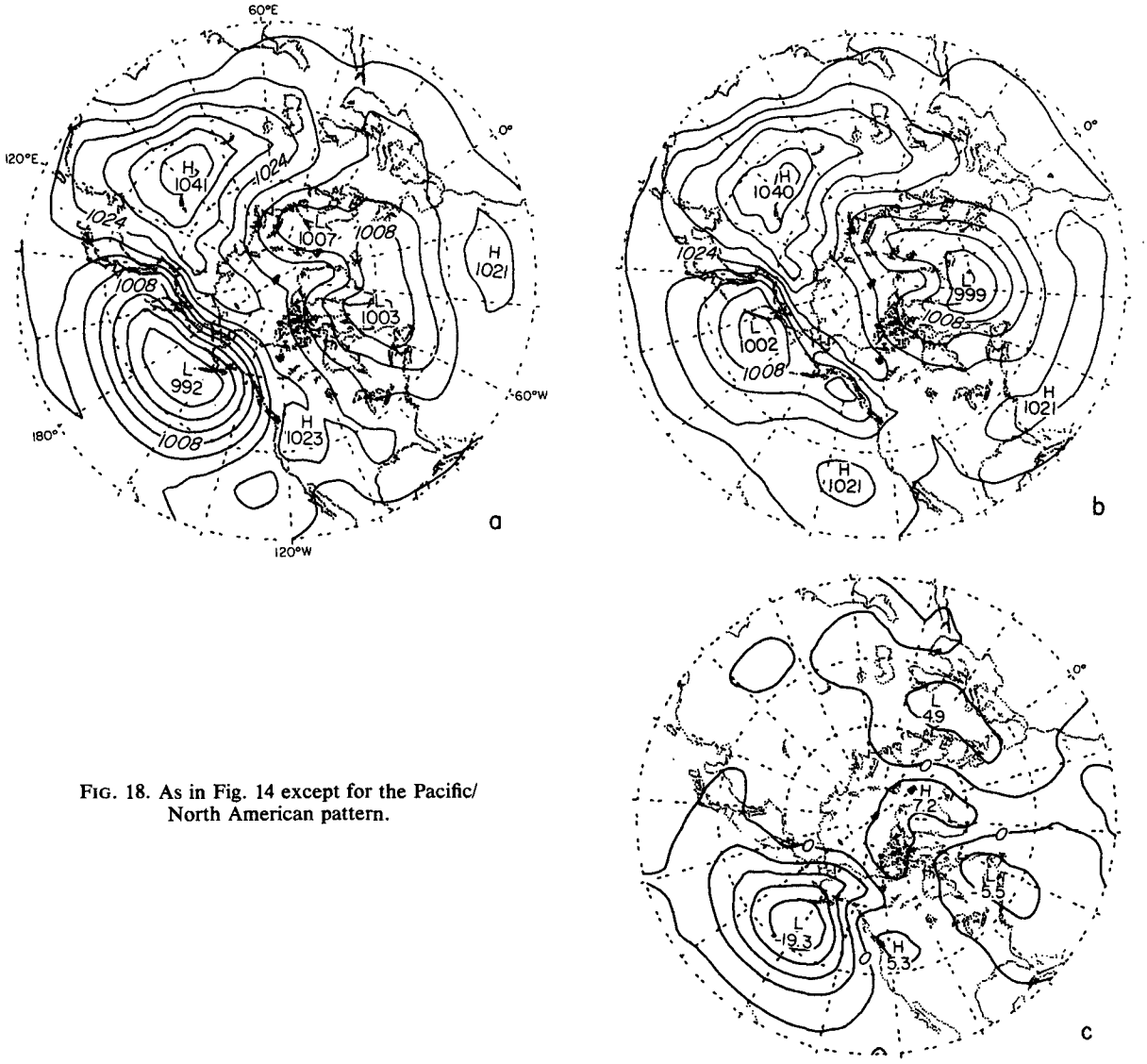

FIG. 18. As in Fig. 14 except for the Pacific/ North American pattern.

d. The western Pacific pattern

One-point correlation maps for the two centers of action of the western Pacific pattern are shown in Fig. 24. This pattern is notable for the strength of the negative correlation between the two centers of action, and for its broad longitudinal extent at low latitudes. It is analogous to the western Atlantic pattern both in terms of its shape and in terms of its position relative to the mean wintertime standing wave pattern.

The composite charts based on the western Pacific pattern index are analogous to the corresponding charts for the western Atlantic pattern, so we have omitted them for the sake of brevity. If we define

$$WP = \tfrac{1}{2}[z^*(60°N, 155°E) - z^*(30°N, 155°E)],$$

the composite charts for positive WP are characterized by a weak Aleutian low (particularly at longitudes west of the data line) and a weak jetstream over Japan, and vice versa. The difference chart for sea-level pressure bears a strong resemblance to Fig. 10, which is indicative of a close association between this pattern and the North Pacific Oscillation in the sea level pressure field identified by Walker and Bliss (1932). The composite thickness pattern is indicative of a cold-core equivalent barotropic structure.

e. The Eurasian pattern

The Eurasian continent is characterized by generally high teleconnectivity at the 500 mb level (Fig. 7b), but an absence of well-defined centers of high

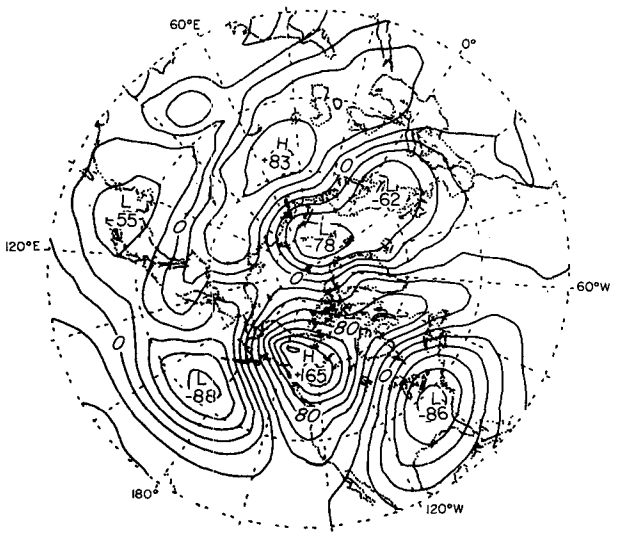

FIG. 19. As in Fig. 15 except for the Pacific/North American pattern.

teleconnectivity which could be used as a basis for identifying patterns. However, three of the patterns that we have already considered appear to involve the Eurasian region, at least to some degree. The eastern Atlantic pattern has one of its primary centers over the Black Sea and a secondary center over Siberia. These features were described in Section 6a. In this subsection we will be mainly concerned with three centers of action over the Eurasian continent which the Pacific/North American and Western Atlantic patterns appear to share in common: one

TABLE 2. Signs of 500 mb height anomalies at the four centers of action of the Pacific/North American pattern. The first symbol for each individual month refers to anomalies at (20°N, 160°W), the second to anomalies at (45°N, 165°W) with sign reversed, the third to anomalies at (55°N, 115°W), and the fourth to anomalies at (30°N, 85°W) with sign reversed. Boldface type refers to anomalies in the upper or lower quintile of the frequency distribution of PNA during the 45-month data set, zeroes to anomalies in the middle quintile. See text for further explanation.

	December	January	February	Winter
1962–63	0 + + +	− + + +	+ + + +	0 + + +
1963–64	+ + + +	+ + 0 0	0 0 0 +	+ + + +
1964–65	0 − − −	0 + + 0	− − − −	− − − −
1965–66	− − − −	+ + 0 +	− − − −	0 − − 0
1966–67	+ + + −	+ 0 0 −	+ 0 − −	+ 0 0 −
1967–68	− − 0 −	− − + −	− + + +	− 0 + +
1968–69	0 − − 0	− − − 0	+ − − +	− − − +
1969–70	+ + + +	+ + + +	+ + + 0	+ + + +
1970–71	− − − −	− − − 0	+ + − −	− − − −
1971–72	− − − −	− − − −	− − − 0	− − − −
1972–73	− 0 − −	+ + + 0	+ 0 + +	+ + 0 −
1973–74	+ + + +	0 0 − −	+ − − 0	+ 0 − −
1974–75	+ 0 0 0	0 − + −	0 − − −	+ − − −
1975–76	− 0 0 +	0 + + +	− − − −	− 0 0 −
1976–77	+ + + +	+ + + +	+ + + +	+ + + +

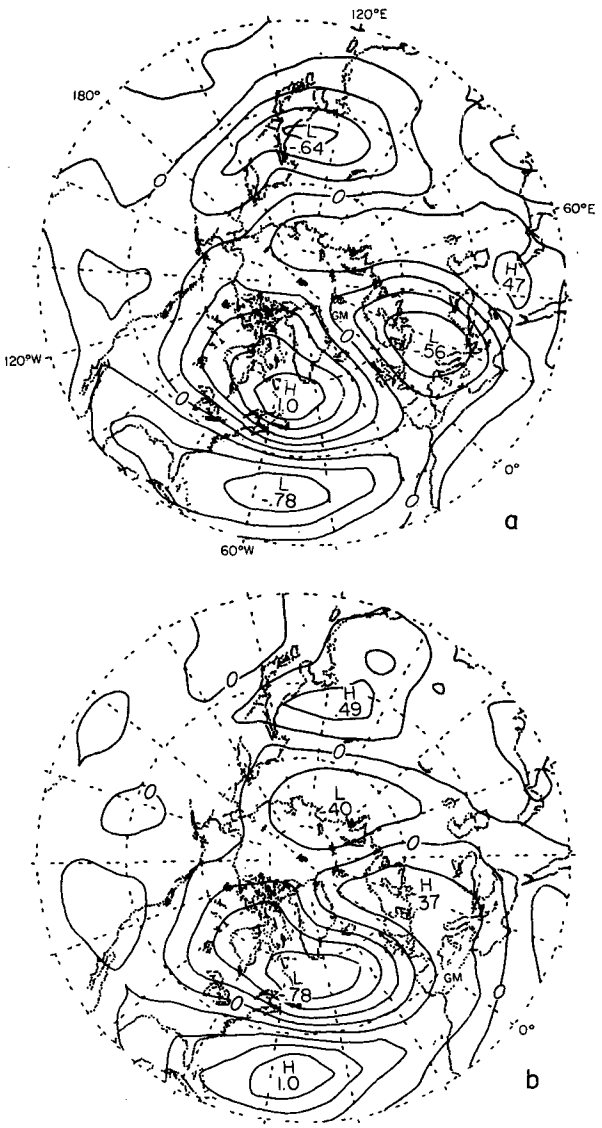

FIG. 20. As in Fig. 12 except for base grid points (a) 55°N, 55°W; (b) 30°N, 55°W.

is located over Scandinavia and Poland (55°N, 20°E), one over Siberia (55°N, 75°E) and one over Japan (40°N, 145°E). The spatial pattern over Eurasia evident on the one-point correlation maps for these three grid points shown in Fig. 25 is similar to the one seen in Figs. 3b, 5a, 16, 17c, 20a and 21c.

Composite charts based on a Eurasian pattern index, defined as

$$EU = -\tfrac{1}{4}z^*\,(55°N, 20°E) + \tfrac{1}{2}z^*\,(55°N, 75°E) - \tfrac{1}{4}z^*\,(40°N, 145°E),$$

have proven to be quite similar to the corresponding charts based on the PNA and WA indices, in terms of the major features over the Eurasian continent, and hence we will not show them here. Dur-

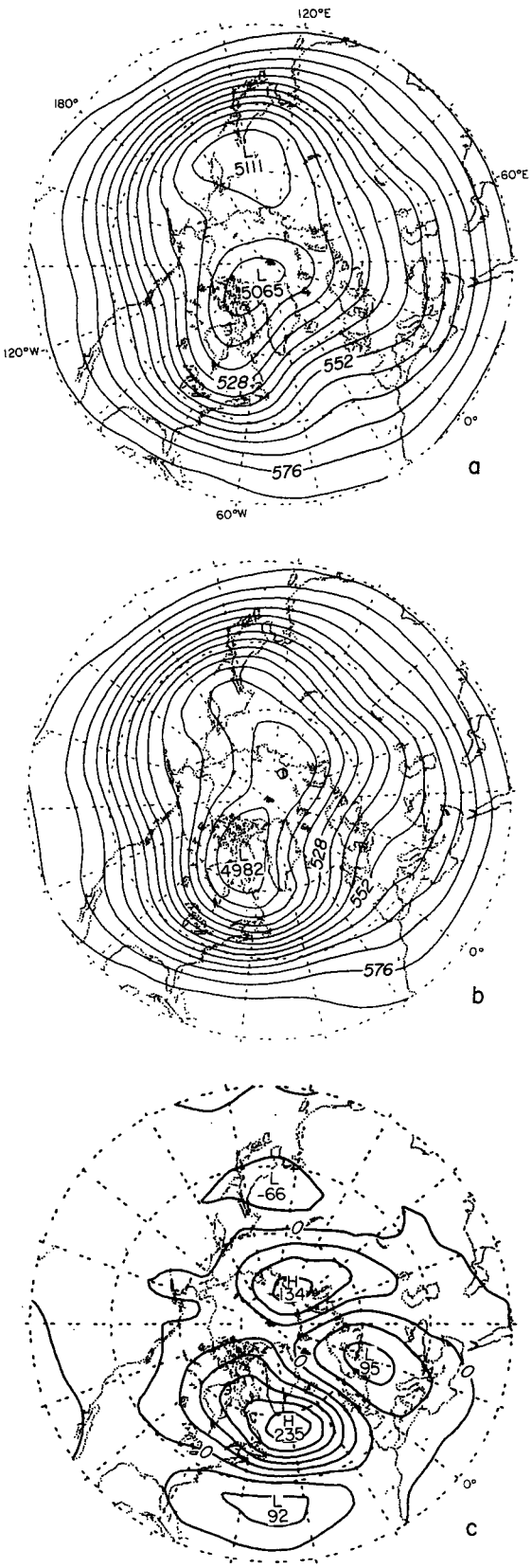

FIG. 21. As in Fig. 13 except for the western Atlantic pattern.

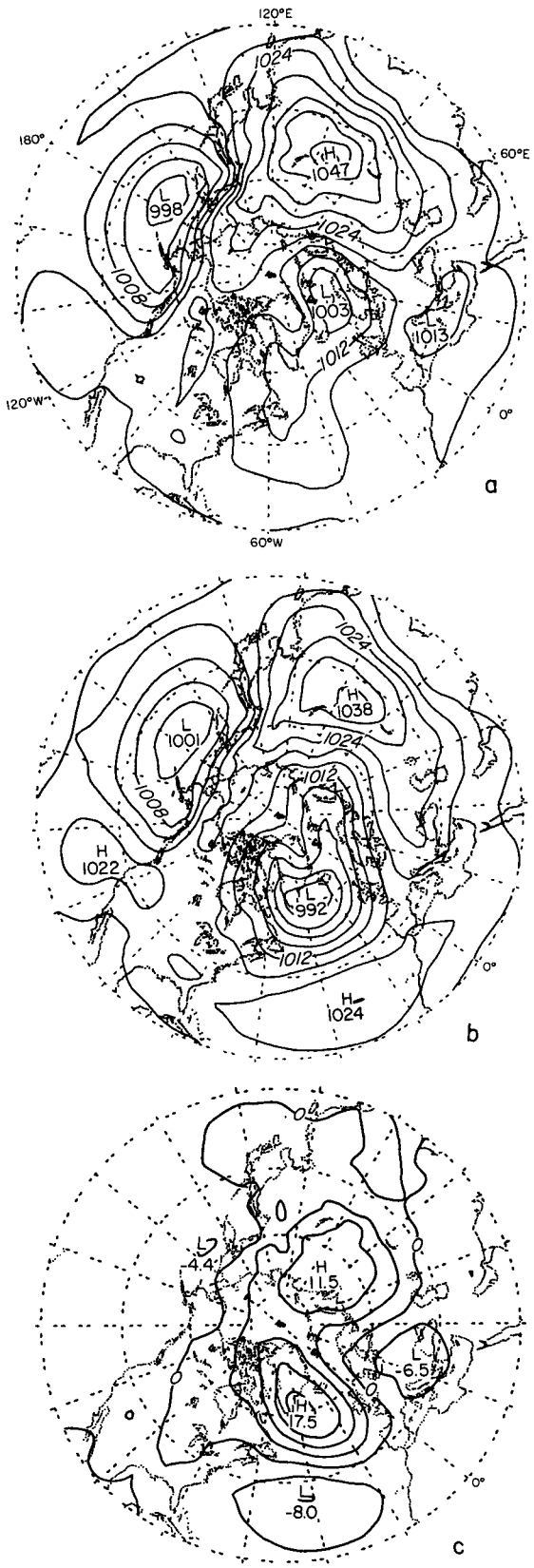

FIG. 22. As in Fig. 14 except for the western Atlantic pattern.

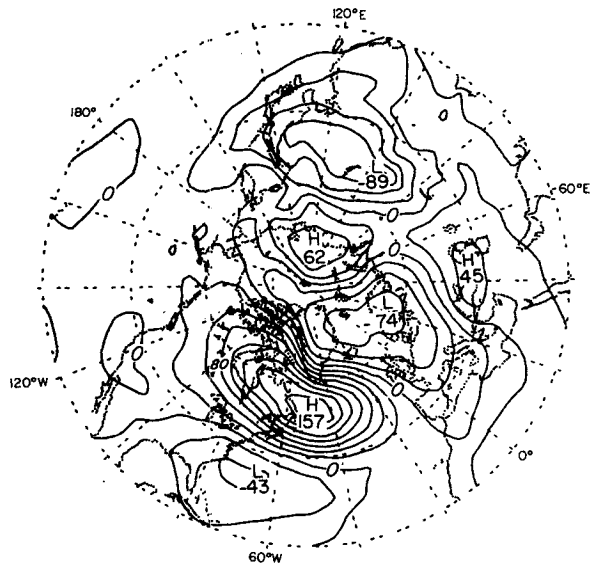

FIG. 23. As in Fig. 15 except for the western Atlantic pattern.

ing months with positive values of EU, the 500 mb flow pattern is characterized by a prominent planetary wave trough located near 30°E (somewhat to the west of its normal climatological position) and on the surface map the Siberian anticyclone is stronger than normal, but largely confined to the region east of the Urals. Temperatures tend to be below normal in most of northern Europe, above normal over much of western Siberia and central Asia, and below normal over Japan and much of China. These same conditions prevail during months with positive values of WA (the index of the western Atlantic pattern) and they are just as evident in the WA composites (Figs. 21a, 22a and 23) as they are in the composites for EU (not shown). In months with negative values of EU, the Eurasian trough in the 500 mb height field is located near 50°E, somewhat to the east of its normal climatological position and the Siberian anticyclones is weaker than normal in the Far East, but it extends westward along 50°N into Europe. These same conditions prevail during months with negative values of WA (Figs. 21b and 22b).

The correspondence between the Eurasian and Pacific/North American patterns is less obvious, but there is some tendency for a positive correlation between their two pattern indices. Hence, for example, the conditions described in connection with positive values of EU are somewhat more likely to prevail during months with positive height anomalies over western Canada than during months with negative height anomalies and vice versa.

f. Summary

In this section, we described five patterns associated with standing oscillations in the winter-time monthly mean mid-tropospheric geopotential height field at middle and high latitudes of the Northern Hemisphere, during winters 1962–63 to 1976–77. Each pattern accounts for a large fraction of the temporal variance of monthly mean data over specific regions of influence. Time series of the five pattern indices are displayed in Table 3. The major centers of action of the five patterns are displayed together in Fig. 26, superimposed upon the climatological mean 500 mb height field for this fifteen winter data sample. The figure was constructed by correlating 500 mb height at each grid-point with each of the five pattern indices and transcribing all the ±0.6 contours onto a single map. The sign of the correlation is indicated at each center; for example, the eastern Atlantic pattern index is positively correlated with 500 mb height west of Great Britain and negatively cor-

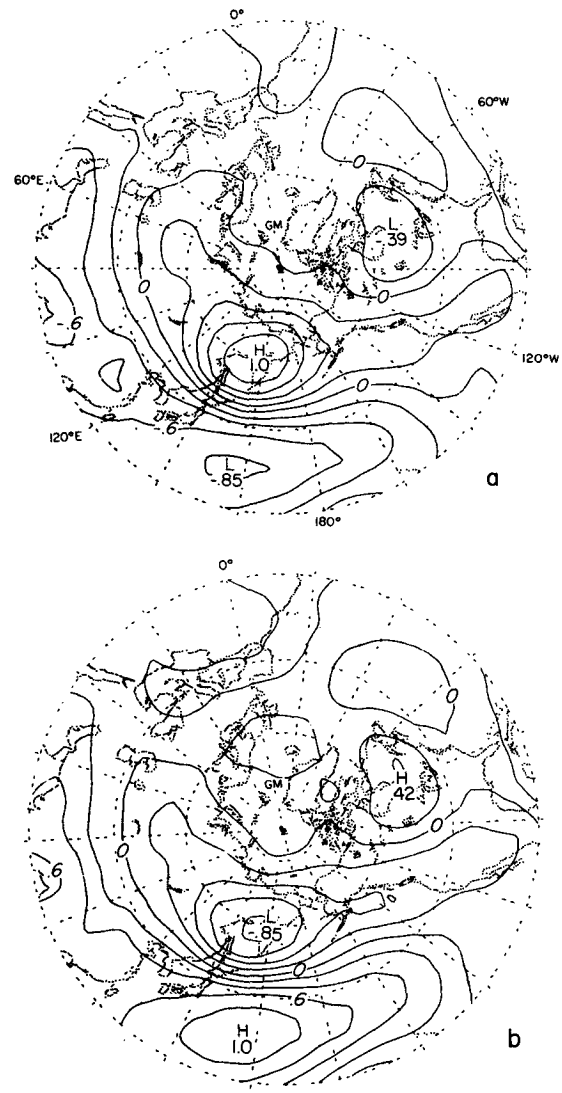

FIG. 24. As in Fig. 12 except for base grid points (a) 60°N, 155°E; (b) 30°N, 155°E.

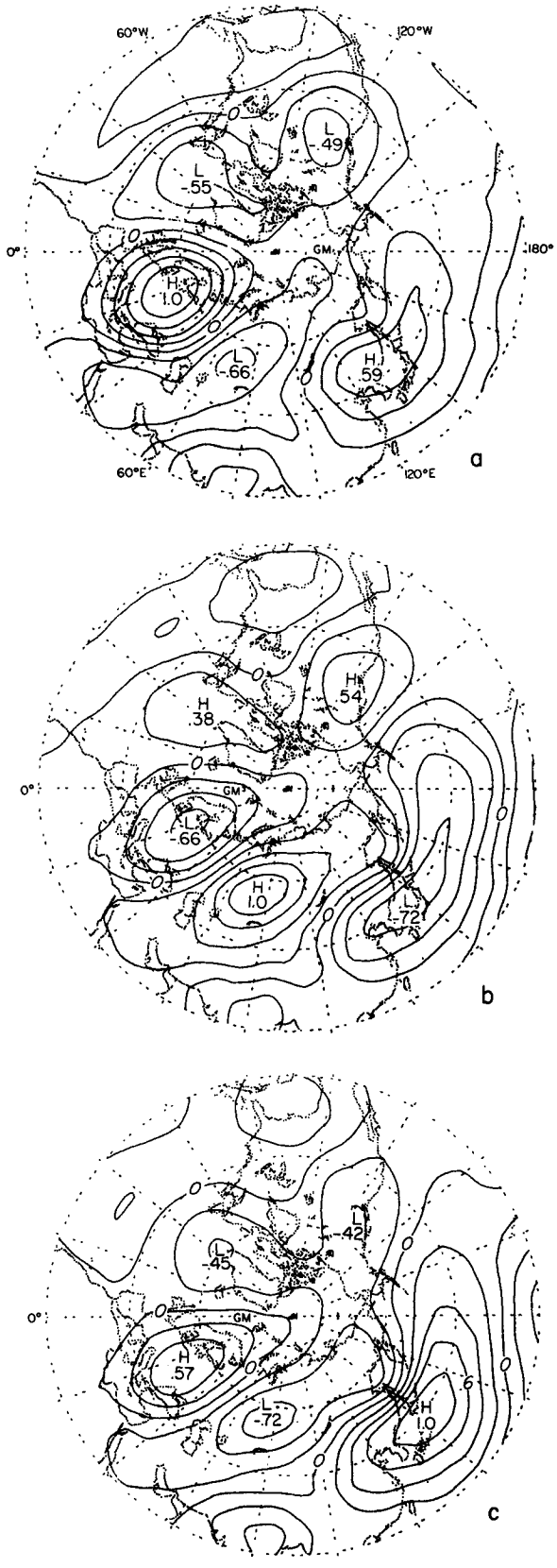

FIG. 25. As in Fig. 12 except for base grid points (a) 55°N, 20°E; (b) 55°N, 75°E; (c) 40°N, 145°E.

related with 500 mb height off the African coast and near the Caspian Sea.

The total area covered by correlations with absolute values ≥ 0.6 includes most of the stippled area in Fig. 7b. We conclude, then, that most of the stronger teleconnections inherent in the monthly mean 500 mb height field over the Northern Hemisphere are incorporated into these five patterns.

There is substantial overlap between several of the patterns, indicating a lack of spatial orthogonality among them. Another measure of the degree of orthogonality between the various patterns, the matrix of correlation coefficients between pairs of the time series of the pattern indices, is shown in Table 4. EA, PNA and WP are nearly mutually orthogonal in the time domain, but each is correlated, to some degree, with WA and EU. PNA and WA are positively correlated with EU, as is to be expected, in view of the redundancies in their respective patterns (as noted in Section 6e). EA and WA are positively correlated, which is reasonable in view of the fact that the regions of high correlation surrounding their pattern centers in the Atlantic occupy partially overlapping geographical locations in Fig. 26; however, the correlation is weak enough to support the definition of the two separate patterns. Likewise, the positive correlation between the PNA and WA patterns is consistent with the fact that two of the centers of the Pacific/North American pattern are adjacent to the two centers of the West Atlantic pattern, and the two patterns share secondary centers in common, which form the Eurasian pattern.

g. Results of eigenvector analysis

The smallness of most of the linear correlations between the pattern indices in Table 4 lends some support to the view that the patterns identified in this section (with the exception of the Eurasian pattern) are unique, or at least that they are not linear combinations of a smaller number of more fundamental patterns. Further evidence in support of this view can be obtained from an inspection of the first four eigenvectors of the normalized covariance matrix **R** (as calculated from the same 15 winter data set), presented in Fig. 27.

In sharp contrast to the leading eigenvector of the sea-level pressure field (Fig. 11b) which is dominated by the zonally symmetric seesaw described in Section 5b, the leading eigenvectors of the 500 mb height field are characterized by strong patterns of a more regional scale. Furthermore, there is a strong correspondence between the shapes of the eigenvector patterns and the teleconnection patterns described in this section:

- The first eigenvector resembles the western Pacific pattern (Fig. 24).
- The second eigenvector is dominated by the

TABLE 3. Time series of 500 mb pattern indices (×100).

Year	EA			PNA			WA			WP			EU		
	Dec	Jan	Feb	Dec	Jan	Feb	Dec	Jan	Feb	Dec	Jan	Feb	Dec	Jan	Feb
1962–63	53	135	−44	56	16	98	−30	63	−69	62	163	142	60	−166	−132
1963–64	−12	106	18	143	37	41	−111	18	−14	−87	−105	−26	82	108	−80
1964–65	−37	−30	213	−92	33	−142	103	32	96	80	−6	37	10	−48	−82
1965–66	−164	−94	−137	−65	67	−96	−55	95	18	−88	−63	−188	−88	−49	69
1966–67	−2	78	−25	58	3	−13	104	−30	−103	118	−122	−53	−52	−74	10
1967–68	126	107	4	78	−54	128	143	29	108	−65	72	178	−86	−94	−108
1968–69	−64	−31	22	−51	−135	−10	−40	161	264	68	−80	−116	156	78	66
1969–70	20	−79	7	150	78	87	108	20	3	−137	47	−57	−83	−08	−87
1970–71	44	−137	91	−95	−78	10	−41	−31	−14	−30	42	104	49	48	12
1971–72	70	−20	−84	−177	−115	−80	−67	−158	−73	−114	−56	86	65	169	122
1972–73	−146	18	79	−50	58	62	−202	−76	54	−16	−92	71	138	153	6
1973–74	57	−135	−82	76	−81	−11	41	−181	−68	−31	230	−08	−86	20	25
1974–75	−22	−38	13	40	−58	−77	16	−84	−101	−52	−70	27	−86	−7	56
1975–76	140	148	43	4	48	−118	101	30	−58	151	11	11	12	−106	173
1976–77	−62	−28	−118	80	179	122	−71	113	−44	142	27	−68	−70	−24	−51

Pacific/North American pattern, including its secondary features over Eurasia (Fig. 16).

- The strongest features in the third eigenvector coincide with the centers of the eastern Atlantic pattern (Fig. 12).
- The fourth eigenvector is closely related to the western Atlantic pattern (Fig. 20).

It should be noted that no less than four eigenvectors are required to convey the essential information on spatial correlations contained in the four (or five if one counts the Eurasian pattern) teleconnection patterns described in this section.

There are some notable differences between the eigenvector patterns and the teleconnection patterns. On the whole, the teleconnection patterns tend to be somewhat more localized, with fewer strong centers of action and they explain a larger fraction of the local variance of 500 mb height in the vicinity of those centers of action. The largest differences between the eigenvector patterns and the teleconnection patterns occur over the Eurasian land mass where there is a large degree of overlap (or non-orthogonality) between the Pacific/North American, western Atlantic and Eurasian teleconnection patterns.

Because of their concise and completely objective mathematical definition, their spatial orthogonality, and their efficiency at explaining the hemispherically integrated normalized variance of the 500 mb height field (48% with the first four eigenvectors) the eigenvector patterns have certain advantages over the teleconnection patterns as a means of displaying the structure of the correlation matrix **R**. The main advantages of the teleconnection patterns are their somewhat more localized spatial structure (which facilitates their interpretation in terms of synoptic or dynamical entities), their greater efficiency at explaining the local variance of the 500

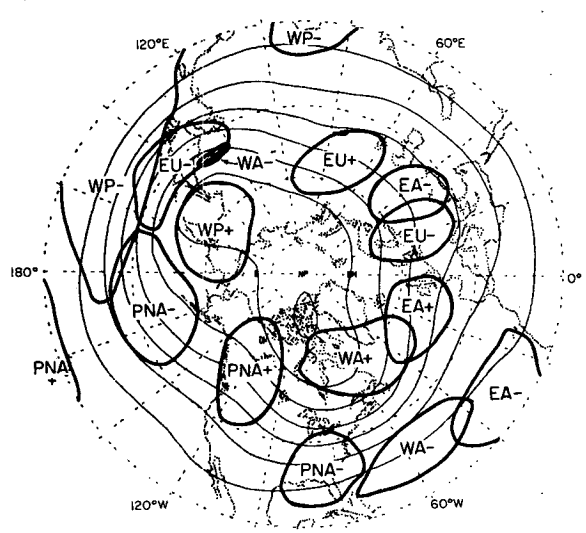

FIG. 26. ±0.6 isopleths of correlation coefficient between each of the five pattern indices and local 500 mb height (heavy lines), superimposed on wintertime mean 500 mb height contours (lighter lines), contour interval 120 m. Based on the same 45-month data set as Fig. 7b. Regions of strong correlation are labeled in terms of the respective pattern indices with which local 500 mb height shows the strongest correlation, and the sign of that correlation is indicated. See text for further details.

TABLE 4. Temporal correlation matrix for the five pattern indices, based on the same 45-month data set as Fig. 7b.

	PNA	WA	WP	EU
EA	−0.01	0.39	0.04	0.24
PNA		0.18	0.07	0.42
WA			−0.07	0.38
WP				0.22

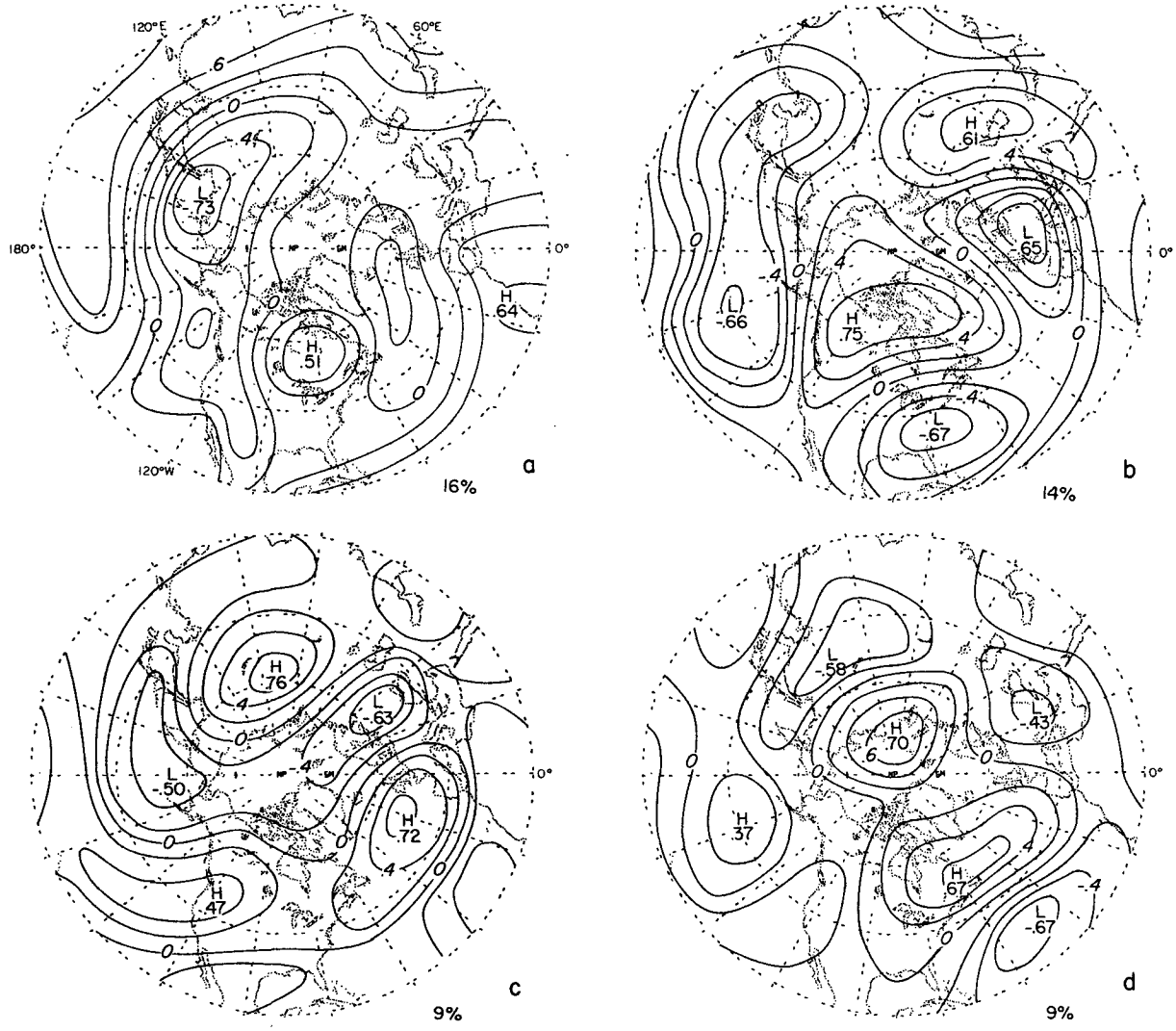

FIG. 27. Horizontal structure of the first four modes of an eigenvector analysis expansion of 500 mb height as computed from the normalized covariance matrix **R**. Based on the same 45 month data set as Fig. 7b. Numbers below each chart indicate the percentage of the hemispherically integrated normalized variance explained by that mode.

mb height field, and the simplicity with which their pattern indices can be computed from 500 mb height data or even, perhaps, from surface pressure and temperature data from a small selection of stations located near centers of action. Horel (1981) has shown that by subjecting the eigenvectors to a VARIMAX rotation, they can be transformed into a set of patterns which much more closely resemble the teleconnection patterns. The rotated patterns are no longer spatially orthogonal, but their coefficients are temporally uncorrelated.

7. Reproducibility in an independent data set

The teleconnection patterns described in the previous two sections were derived from correlation matrices based on a 15-winter data sample which represents about half the total available record of hemispheric gridded upper air data. We will now briefly describe the results of our attempts to determine the reproducibility of these patterns in an independent data set consisting of 39 winter months: the Decembers, Januarys and Februarys of the winters beginning with 1949–50 and ending with 1961–62. For these earlier years the data for 700 mb height are more complete than those for 500 mb height. Having verified by direct calculations on the 1962–63 to 1976–77 data set that the teleconnection patterns at the 500 and 700 mb levels are very similar, we took the liberty of using 700 mb data in place of 500 mb data in our analysis of the earlier, 13-winter period of record.

Fig. 28 shows 700 mb one-point correlation maps for a selection of grid points which occupy key

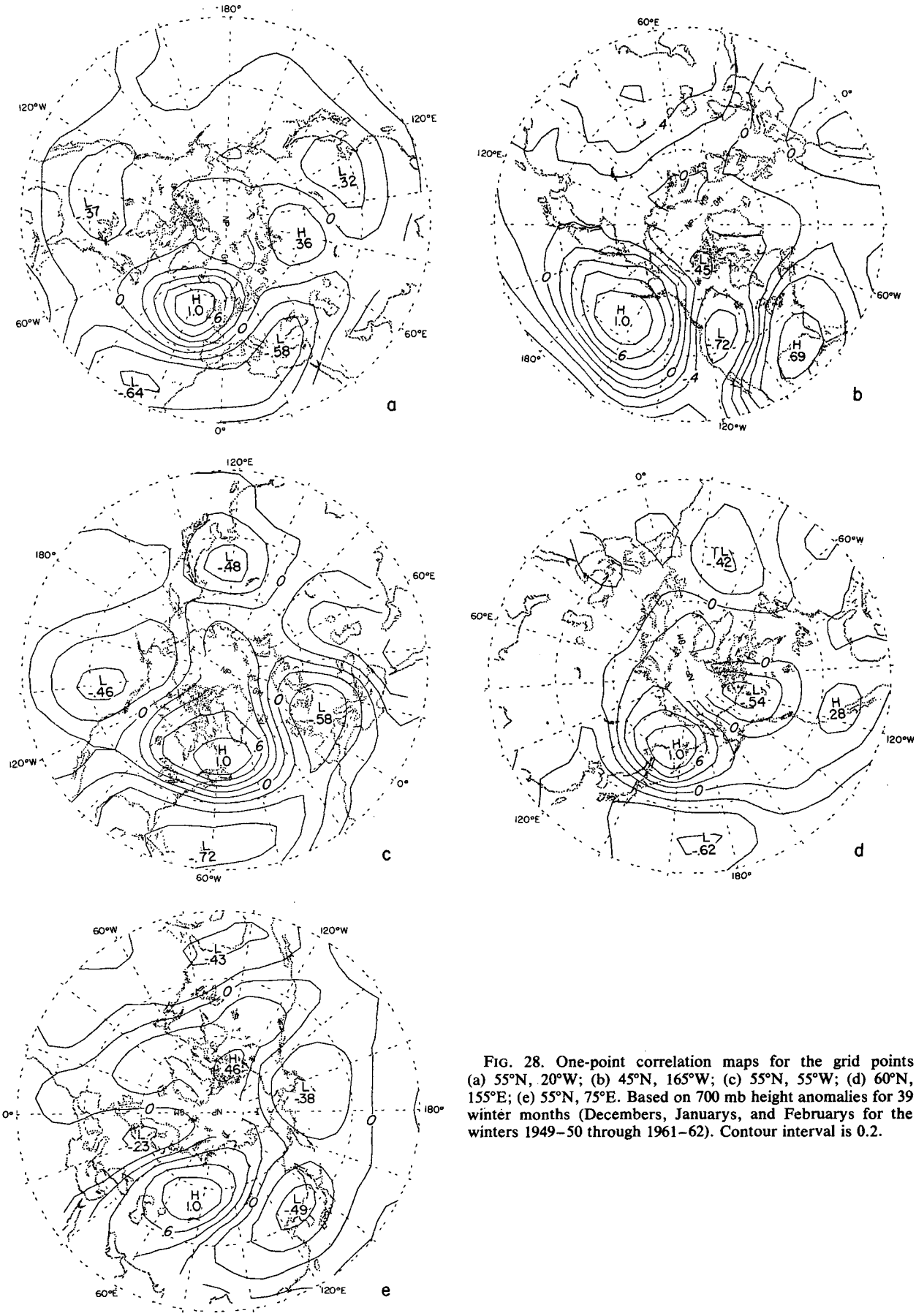

FIG. 28. One-point correlation maps for the grid points (a) 55°N, 20°W; (b) 45°N, 165°W; (c) 55°N, 55°W; (d) 60°N, 155°E; (e) 55°N, 75°E. Based on 700 mb height anomalies for 39 winter months (Decembers, Januarys, and Februarys for the winters 1949–50 through 1961–62). Contour interval is 0.2.

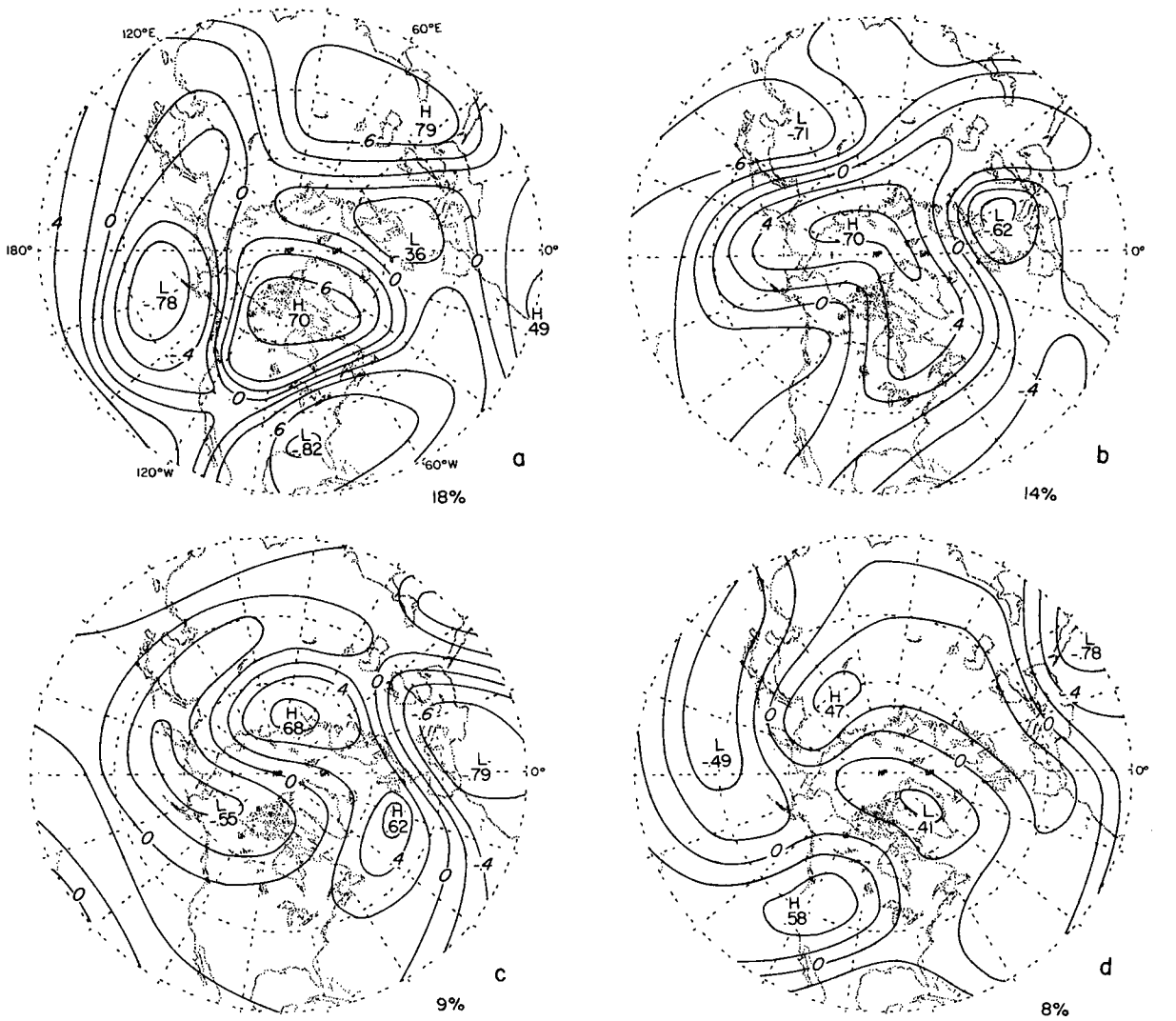

FIG. 29. As in Fig. 27 except for the same 39-month data set as Fig. 28.

positions in the five teleconnection patterns described in the previous section. All the patterns appear to be qualitatively reproducible in the independent data set, but most of them show some diminution in sharpness.

A more stringent test of the similarity of the correlation matrix **R** in the two data samples is the reproducibility of the leading eigenvectors described in the previous section in the independent sample. Fig. 29 shows the first four eigenvectors of the 700 mb correlation matrix for the 1949–50 to 1961–62 data set. Eigenvector number 1 bears some resemblance to the Pacific/North American pattern, and it also contains elements of the Western Atlantic pattern. The second and fourth eigenvectors exhibit certain features reminiscent of Figs. 27d and 27c, respectively, but they do not look particularly like any of the patterns described in the previous section. The third eigenvector bears some resemblance to the Eastern Atlantic pattern. Evidently, the eigenvector patterns are considerably less reproducible in the independent data set than are the one-point correlation maps.

Still another indication of the similarities and differences between the two data sets can be obtained from a comparison of the teleconnectivity maps shown in Figs. 7 and 30. The two strongest teleconnection patterns in the sea level pressure distribution, as inferred from Fig. 7a, appear to be qualitatively reproducible in the independent data set. The results for the 700 and 500 mb levels are more ambiguous. Analogs of the Pacific/North American and western Atlantic patterns are clearly evident in the independent data set (Fig. 30b), but their centers occur at slightly different locations than those in Fig. 7b. Conspicuously absent in the independent data set is an analog of the western Pacific pattern, spatially orthogonal to the Pacific/North American pattern. Evidence in support of an analog to the eastern Atlantic pattern is marginal,

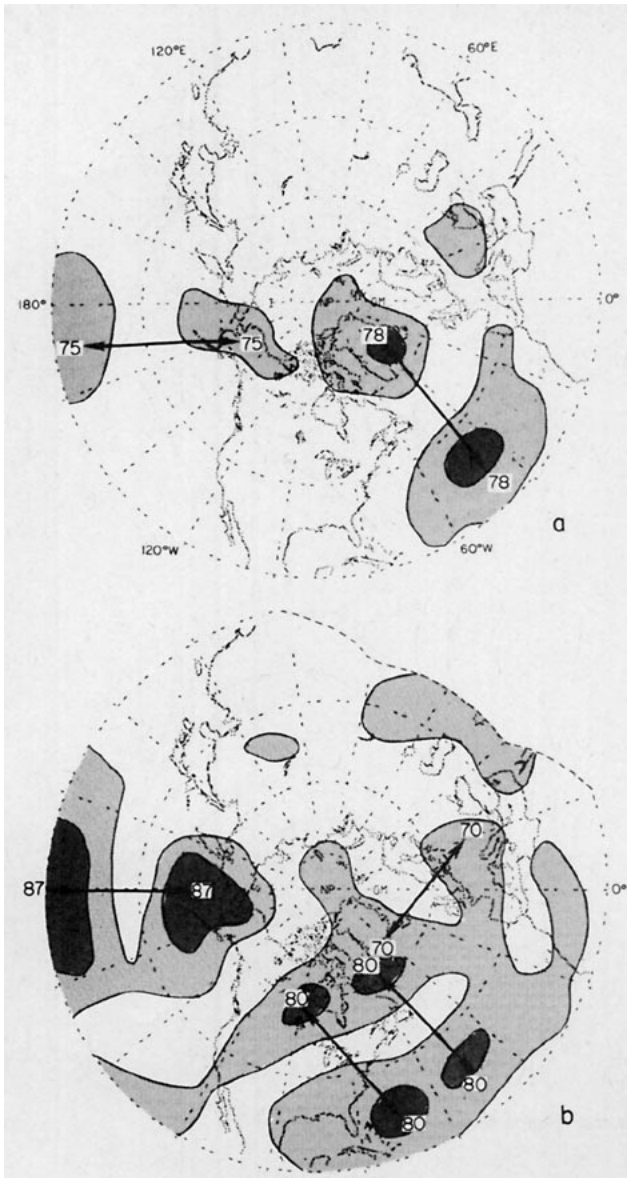

FIG. 30. As in Fig. 7 except for the same 39-month data set as Fig. 28: (a) sea-level pressure, (b) 700 mb height.

at best. The general level of teleconnectivity over the Eurasian land mass is considerably lower in the 1949–50 to 1961–62 data set than in the 1962–63 to 1976–77 data set.

At least two factors may contribute to the observed differences between the normalized correlation matrices derived from the two data sets. Many (or perhaps even all) of the differences may simply be a reflection of sampling fluctuations: a 15-winter data set may be adequate for obtaining qualitatively reproducible samples of the structure of the individual columns of the correlation matrix **R** (the one-point correlation maps), but inadequate for obtaining reproducible samples of the teleconnectivity vector **T**, or the eigenvectors of **R**. It is also possible that the differences are a result of systematic local biases in the 700 mb height analyses during parts of the earlier data sample. Efforts are currently underway to determine the adequacy of the sample size used in this study and to ascertain the reliability of the 700 mb height analyses for the winters during the 1950's.

8. Discussion

The results of this study indicate that the major teleconnection patterns in the geopotential height field during the Northern Hemisphere winter season are of two different types:

1) A zonally symmetric, global-scale "seesaw" between polar and temperate latitudes, which is most clearly defined in the sea level pressure field. This zonally symmetric teleconnection pattern was first pointed out by Lorenz (1951), and it has been subsequently noted by Brier (1968), Kutzbach (1970) and others.

2) Patterns of a more regional scale, more clearly defined at mid-tropospheric levels than at the earth's surface. The most reproducible of these patterns are what we have referred to as the Pacific/North American pattern, which has been previously noted by Namias and collaborators, and the Western Atlantic pattern, which is closely related to the so-called North Atlantic Oscillation identified by Walker and Bliss (1932). At mid-tropospheric levels the horizontal scale and spatial orientation of the patterns resemble the steady, linear response of a spherical atmosphere to thermal and/or orographic forcing (Hoskins and Karoly, 1981). The observed patterns are characterized by an equivalent barotropic vertical structure. Their horizontal structure at mid-tropospheric levels tends to be wavelike with multiple centers of action, whereas the corresponding patterns of the earth's surface tend to be more localized; in these respects the observed patterns also resemble the linear solutions obtained by Hoskins and Karoly. The geographical location of the patterns, depicted in Fig. 26, appears to bear some relation to the major features of the wintertime mean planetary wave pattern: e.g., dipole patterns straddle both the major jet streams and the Eurasian pattern has the same southwest–northeast tilt as the upper level trough in that sector of the hemisphere.

At mid-tropospheric levels the regional scale patterns are dominant, whereas at the earth's surface the zonally symmetric pattern and the regional patterns appear to be of roughly comparable importance. The coexistence of the two kinds of patterns in the sea level pressure field might account for the rather weak temporal correlations between the depths of the Icelandic and Aleutian lows, despite the consistent negative correlations between

these two regions in the regional scale patterns. Perhaps the regional scale patterns would stand out more clearly in the sea level pressure data if the zonally symmetric fluctuations were first removed.

There are a number of observational questions concerning the nature, causes, and dynamical implications of these patterns which have not been addressed in the present study, but are currently under active consideration:

- What is the frequency dependence of the structure of the correlation matrix **R**? Is it essentially the same for winter-to-winter variability as for month-to-month variability within the same winter? Do the same structures show up in daily data or in 5-day average data?
- Are the frequency spectra of the pattern indices characterized by a higher level of autocorrelation than the frequency spectra of geopotential height at individual gridpoints? Do they show evidence of enhanced power at periods on the order of a few weeks, which might be indicative of vacillation cycles?
- Do similar teleconnection patterns exist in other seasons or in the Southern Hemisphere? Do they exist in the "climates" generated by general circulation models?
- Is the signature of the teleconnection patterns apparent in the stratospheric circulation? Are any of the patterns related to stratospheric warmings?
- Are the year-to-year fluctuations in hemispherically averaged surface temperatures reported by Yamamoto and Hoshiai (1979) and others due to fluctuations in the polarity and strength of the various teleconnection patterns in different years or are they due to other mechanisms, such as volcanic activity, which might be expected to produce a rather uniform geographical distribution of temperature changes?
- How should teleconnection patterns be viewed in relation to synoptic patterns associated with blocking? Is it most useful to think of one set of patterns as a subset of the other, or would it be better to define them in such a way that they are mutually exclusive?
- Do the extratropical Northern Hemisphere patterns described in the paper extend into the tropics or even into the Southern Hemisphere extratropics? Rogers and van Loon (1979) and Meehl and van Loon (1979) have, in fact, shown evidence that the strength of the surface westerlies in the North Atlantic (which is related to our "Eastern and Western Atlantic patterns") is positively correlated with the strength of the Atlantic tradewinds. Walker and Bliss (1932) and Wright (1978) have shown that the Southern Oscillation in sea level pressure in the Southern Hemisphere tropics has a distinct signature in the Northern Hemisphere extratropics which contains elements of our western Pacific and Pacific/North American patterns. The latter relationships are discussed further in a paper by Horel and Wallace (1981) in this issue.

Acknowledgments. We wish to thank Grant Branstator for helpful discussions and John Horel and Harold J. Edmon for their help and guidance in certain aspects of the data processing and calculations. Some of the computations were performed at the Computer Facility of the National Center for Atmospheric Research. The research was supported under the Climate Dynamics Program in the Atmospheric Sciences Division of the National Science Foundation under Grant 78-07369.

REFERENCES

Bjerknes, J., 1969: Atmospheric teleconnections from the equatorial Pacific. *Mon. Wea. Rev.*, **97**, 162–172.

Blackmon, M. L., R. A. Madden, J. M. Wallace and D. S. Gutzler, 1979: Geographical variations in the vertical structure of geopotential height fluctuations. *J. Atmos. Sci.*, **36**, 2450–2466.

Brier, G. W., 1968: Long range prediction of the zonal westerlies and some problems in data analysis. *Rev. Geophys.*, **6**, 525–551.

Defant, A., 1924: Die Schwankungen der atmospherischen Zirkulation über dem Nordatlantischen Ozean im 25-jährigen Zeitraum 1881–1905. *Geogr. Ann.*, **6**, 13–41.

Dickson, R. R., and J. Namias, 1976: North American influences on the circulation and climate of the North Atlantic sector. *Mon. Wea. Rev.*, **104**, 1255–1265.

Ebdon, R. A., 1975: The quasi-biennial oscillation and its association with tropospheric circulation patterns. *Meteor. Mag.*, **104**, 282–297.

Hildebrandsson, H. H., 1897: Quelques recherches sur les centres d'action de l'atmosphère. *Kon. Svenska Vetens. Akad. Handl.*, No. 29, 36 pp.

Horel, J. D., 1981: A rotated principal component analysis of the Northern Hemisphere 500 mb height field. Submitted to *Mon. Wea. Rev.*

——, and J. M. Wallace, 1981: Planetary-scale atmospheric phenomena associated with the Southern Oscillation. *Mon. Wea. Rev.*, **109**, 813–829.

Hoskins, B. J., and D. Karoly, 1981: The steady, linear response of a spherical atmosphere to thermal and orographic forcing. *J. Atmos. Sci.*, **38** (in press).

Klein, W. H., 1952: Some empirical characteristics of long waves on monthly mean charts. *Mon. Wea. Rev.*, **80**, 203–219.

——, B. M. Lewis, C. W. Crockett and I. Enger, 1960: Application of numerical prognostic heights to surface temperature forecasts. *Tellus*, **12**, 378–392.

Krueger, A. F., and T. I. Gray, 1969: Long-term variations in equatorial circulation and rainfall. *Mon. Wea. Rev.*, **97**, 700–711.

Kutzbach, J. E., 1970: Large-scale features of monthly mean Northern Hemisphere anomaly maps of sea-level pressure. *Mon. Wea. Rev.*, **98**, 708–716.

Lorenz, E. N., 1951: Seasonal and irregular variations of the Northern Hemisphere sea-level pressure profile. *J. Meteor.*, **8**, 52–59.

Meehl, G. A., and H. van Loon, 1979: The seesaw for winter temperatures between Greenland and northern Europe. Part III. Teleconnections with lower latitudes. *Mon. Wea. Rev.*, **79**, 1095–1106.

Namias, J., 1951: The great Pacific anticyclone of the winter 1948–50: A case study in the evolution of climatic anomalies. *J. Meteor.*, **8**, 251–261.

——, 1978: Multiple causes of the North America abnormal winter 1976–77. *Mon. Wea. Rev.*, **106**, 279–295.

Quiroz, R. S., 1977: The tropospheric-stratospheric polar vortex breakdown of January 1977. *Geophys. Res. Lett.*, **4**, 151–154.

Ramage, C., 1975: Preliminary discussion of the 1972–73 El Niño. *Bull. Amer. Meteor. Soc.*, **56**, 234–242.

Rogers, J. C., 1981: The North-Pacific Oscillation. *J. Climatol.*, **1** (in press).

——, and H. van Loon, 1979: The seesaw in winter temperatures between Greenland and Northern Europe. Part II: Some atmospheric and oceanic effects in middle and high latitudes. *Mon. Wea. Rev.*, **107**, 509–519.

Rowntree, P. R., 1972: The influence of tropical east Pacific Ocean temperatures on the atmosphere. *Quart. J. Roy. Meteor. Soc.*, **98**, 290–321.

Sawyer, J. S., 1970: Observational characteristics of atmospheric fluctuations with a time scale of a month. *Quart. J. Roy. Meteor. Soc.*, **96**, 610–625.

Thiebaux, H. J., 1977: Extending estimation accuracy with anisotropic interpolation. *Mon. Wea. Rev.*, **105**, 691–699.

Troup, A. J., 1965: The Southern Oscillation. *Quart. J. Roy. Meteor. Soc.*, **98**, 490–506.

van Loon, H., and J. C. Rogers, 1978: The seesaw in winter temperatures between Greenland and Northern Europe. Part I: General description. *Mon. Wea. Rev.*, **106**, 296–310.

Walker, G. T., and E. W. Bliss, 1932: World Weather V. *Mem. Roy. Meteor. Soc.*, **4**, 53–84.

Wright, P. B., 1978: The Southern Oscillation. *Climatic Change and Variability*, A. B. Pittock, L. A. Frakes, D. Jenssen, J. A. Patterson and J. W. Zillman Eds., Cambridge University Press, 180–185.

Yamamoto, R., and M. Hoshiai, 1979: Recent change of the Northern Hemisphere mean surface air temperature estimated by optimum interpolation. *Mon. Wea. Rev.*, **107**, 1239–1244.